Article

Non-canonical Shedding of TNFα by SPPL2a Is Determined by the Conformational Flexibility of Its Transmembrane Helix

Charlotte Spitz, Christine Schlosser, Nadja Guschtschin-Schmidt, ..., Dieter Langosch, Claudia Muhle-Goll, Regina Fluhrer

regina.fluhrer@med.uni-augsburg.de

HIGHLIGHTS

SPPL2a acts a non-canonical sheddase on TNFα

Increased conformational flexibility of TNFα enhances non-canonical shedding

Decreased conformational flexibility of TNFα reduces non-canonical shedding

iScience

Article

Non-canonical Shedding of TNFα by SPPL2a Is Determined by the Conformational Flexibility of Its Transmembrane Helix

Charlotte Spitz,[1] Christine Schlosser,[1] Nadja Guschtschin-Schmidt,[2] Walter Stelzer,[3] Simon Menig,[4] Alexander Götz,[5] Martina Haug-Kröper,[1] Christina Scharnagl,[4] Dieter Langosch,[3] Claudia Muhle-Goll,[2] and Regina Fluhrer[1,6,7,*]

SUMMARY

Ectodomain (EC) shedding defines the proteolytic removal of a membrane protein EC and acts as an important molecular switch in signaling and other cellular processes. Using tumor necrosis factor (TNF)α as a model substrate, we identify a non-canonical shedding activity of SPPL2a, an intramembrane cleaving aspartyl protease of the GxGD type. Proline insertions in the TNFα transmembrane (TM) helix strongly increased SPPL2a non-canonical shedding, while leucine mutations decreased this cleavage. Using biophysical and structural analysis, as well as molecular dynamic simulations, we identified a flexible region in the center of the TNFα wildtype TM domain, which plays an important role in the processing of TNFα by SPPL2a. This study combines molecular biology, biochemistry, and biophysics to provide insights into the dynamic architecture of a substrate's TM helix and its impact on non-canonical shedding. Thus, these data will provide the basis to identify further physiological substrates of non-canonical shedding in the future.

INTRODUCTION

Ectodomain (EC) shedding is a non-reversible posttranslational modification that controls the level and function of various membrane proteins by proteolytic removal of their extracellular/luminal domains (Lichtenthaler et al., 2018). Canonical sheddases commonly cleave single-span transmembrane (TM) proteins in the luminal juxtamembrane (JM) domain with a short distance to the TM domain (Ehlers and Riordan, 1991). This results in release of a soluble EC, which can induce signaling in neighboring or even far distant cells by interacting with cell surface receptors. Intramembrane proteases catalyze the hydrolysis of peptide bonds in the plane of the membrane and typically release a short secreted peptide and an intracellular fragment (ICD), which may translocate to the nucleus and induce signaling in the substrate-expressing cell (Friedmann et al., 2006; Lichtenthaler et al., 2018; Mentrup et al., 2015; Nagase and Nakayama, 2013).

Signal peptide peptidase (SPP) and its homologs, the SPP-like proteases (SPPLs), are aspartyl intramembrane proteases that are closely related to presenilins, which form the active subunit of the γ-secretase complex (Grigorenko et al., 2002; Ponting et al., 2002; Weihofen et al., 2002). The human genome encodes five members of the SPP/SPPL family: SPP, SPPL2a, SPPL2b, SPPL2c, and SPPL3 (Grigorenko et al., 2002; Ponting et al., 2002; Weihofen et al., 2002). Based on a conserved GxGD motif in one of their TM domains, these proteases are also referred to as GxGD proteases (Haass and Steiner, 2002). The GxGD motif harbors one of the two catalytic aspartyl residues required for proteolytic activity (Bardy et al., 2003; Haass and Steiner, 2002; LaPointe and Taylor, 2000). The second catalytic aspartyl residue is part of a (Y/F)D motif located in the TM domain N-terminal of the GxGD motif. In contrast to presenilins that exclusively cleave type I TM domains (N_{out}) (Hemming et al., 2008; Kopan and Ilagan, 2004), SPP/SPPLs are selective toward TM segments in type II (N_{in}) orientation (Chen et al., 2014; Friedmann et al., 2004; Nyborg et al., 2004; Weihofen et al., 2002). While currently more than 140 substrates have been assigned to the two human presenilins (Güner and Lichtenthaler, 2020), only about 30 human substrates are known for all five SPP/SPPL family members (Mentrup et al., 2017, 2019; Papadopoulou et al., 2019).

[1]Biochemistry and Molecular Biology, Institute of Theoretical Medicine, Medical Faculty, University of Augsburg, Universitätsstrasse 2, 86159 Augsburg, Germany

[2]Karlsruhe Institute of Technology, Institute for Biological Interfaces 4, 76344 Eggenstein- Leopoldshafen, Germany and Karlsruhe Institute of Technology, Institute of Organic Chemistry, 76131 Karlsruhe, Germany

[3]Lehrstuhl für Chemie der Biopolymere, Technische Universität München, Weihenstephaner Berg 3, 85354 Freising, Germany

[4]Physics of Synthetic Biological Systems, Technische Universität München, Maximus-von-Imhof Forum 4, 85340 Freising, Germany

[5]Present Address: Leibniz Supercomputing Centre, Boltzmannstr. 1, 85748 Garching, Germany

[6]DZNE – German Center for Neurodegenerative Diseases, Feodor-Lynen-Str 17, 81377 Munich, Germany

[7]Lead Contact

*Correspondence:
regina.fluhrer@med.uni-augsburg.de

https://doi.org/10.1016/j.isci.2020.101775

The so far known SPPL2a and SPPL2b substrates are mostly single-span TM proteins that are subject to regulated intramembrane proteolysis (RIP), a two-step process that starts with EC shedding followed by an intramembrane cleavage (Lichtenthaler et al., 2018). It is believed that in this context intramembrane proteolysis occurs constitutively after canonical shedding has occurred, and, thus, EC shedding is the regulating step in this process (Lichtenthaler et al., 2018).

A very well-characterized RIP substrate is tumor necrosis factor α (TNFα). Its canonical shedding is catalyzed by a disintegrin and metalloprotease 17 (ADAM17), also known as TNFα-converting enzyme, and other membrane-bound metalloproteases (Black et al., 1997; McGeehan et al., 1994). The soluble TNFα extracellular domain (sTNFα) acts as a ligand for the TNFα receptors 1 and 2 that can either induce apoptosis or cell survival via several pathways (Black et al., 1997; McGeehan et al., 1994). A short N-terminal TNFα fragment (TNFα NTF) remains within the plasma membrane of the TNFα-expressing cell and can be processed further by SPPL2a or SPPL2b (Fluhrer et al., 2006; Friedmann et al., 2006). Intramembrane proteolysis of the TNFα NTF starts with initial cleavages at the C-terminal membrane boundary releasing TNFα C-peptide into the extracellular space. Subsequently, multiple processive intramembrane cleavages finally result in release of TNFα ICD into the cytosol (Figure 1A). While TNFα ICD has been suggested to induce IL-12 production in activated dendritic cells (Friedmann et al., 2006), the function of the TNFα C-peptide remains enigmatic.

SPPL2b and presenilins only efficiently cleave their substrates either after a preceding EC shedding or if the substrates' EC is naturally short (Güner and Lichtenthaler, 2020; Martin et al., 2009). Membrane proteins with an EC length exceeding 60 amino acids are not recognized as bona fide substrates by these proteases (Martin et al., 2008; Struhl and Greenwald, 1999). Based on this, it was concluded that members of the GxGD aspartyl proteases do not accept substrates with bulky long EC. However, just recently, SPPL3 has been demonstrated to act as a non-canonical sheddase as it accepts full-length (FL) glycosyltransferases and glycosidases directly as substrates and by that regulates the glycosylation status of many cellular glycoproteins including those of the extracellular matrix (Kuhn et al., 2015; Voss et al., 2014). Also, the cleavage of naturally short substrates by presenlin has been recently categorized as a non-canonical shedding event (Lichtenthaler et al., 2018). One example of such a non-canonical shedding is the processing of the B-cell maturation antigen which controls plasma cells in the bone marrow and yields a potential biomarker for B-cell involvement in human autoimmune diseases (Laurent et al., 2015), highlighting the biological relevance of non-canonical shedding. However, so far, it is not known how intramembrane proteases recognize and process their substrates for non-canonical shedding.

Other than most soluble proteases, intramembrane proteases in the context of RIP typically do not recognize their substrates by consensus sequences but rather seem to sense structural properties, including the dynamics of the substrate's TM helix (Hitzenberger et al., 2020; Langosch et al., 2015; Langosch and Steiner, 2017). For instance, cleavage of the C-terminal β-amyloid precursor protein (APP) fragment (C99) by presenilin is influenced by the local helical flexibility at the G37G38 hinge located in the N-terminal half of its TM domain (Barrett et al., 2012; Götz et al., 2019b; Scharnagl et al., 2014). It has been proposed that a flexible TM helix facilitates translocation of a substrate from an initial binding site of the enzyme toward its catalytic center (Langosch et al., 2015; Langosch and Steiner, 2017). Furthermore, helix flexibility around the substrate's initial cleavage sites may facilitate its local unfolding, prior to endoproteolysis as suggested by mutational and structural studies (Fernandez et al., 2016; Sato et al., 2009; Zhou et al., 2019). In case of SPP/SPPL substrates, studies on a viral SPP substrate (Lemberg and Martoglio, 2002) and on the SPPL2b substrate Bri2 (Fluhrer et al., 2012) indicate that specific glycine residues in the TM domain of these substrates enhance their cleavability by SPP or SPPL2b, respectively.

Yet, due to lack of detailed studies on further substrates, it is not clear whether the dynamical properties of the substrate's TM helix are generally decisive to qualify a type II TM protein as SPPL2 substrate. This prompted us to ask whether processing of TNFα by SPPL2a is similar to that observed for its close homolog SPPL2b (Martin et al., 2009), if SPPL2 proteases would also be able to directly cleave TNFα FL and, if so, what primary structure determinants and structural properties of the TNFα TM domain would affect this non-canonical shedding.

RESULTS

SPPL2a Mediates Non-canonical Shedding of TNFα

SPPL2a and SPPL2b have been shown earlier to be capable of processing the TNFα NTF that remains in the plasma membrane after shedding by ADAM10/17 (Fluhrer et al., 2006; Friedmann et al., 2006). To test
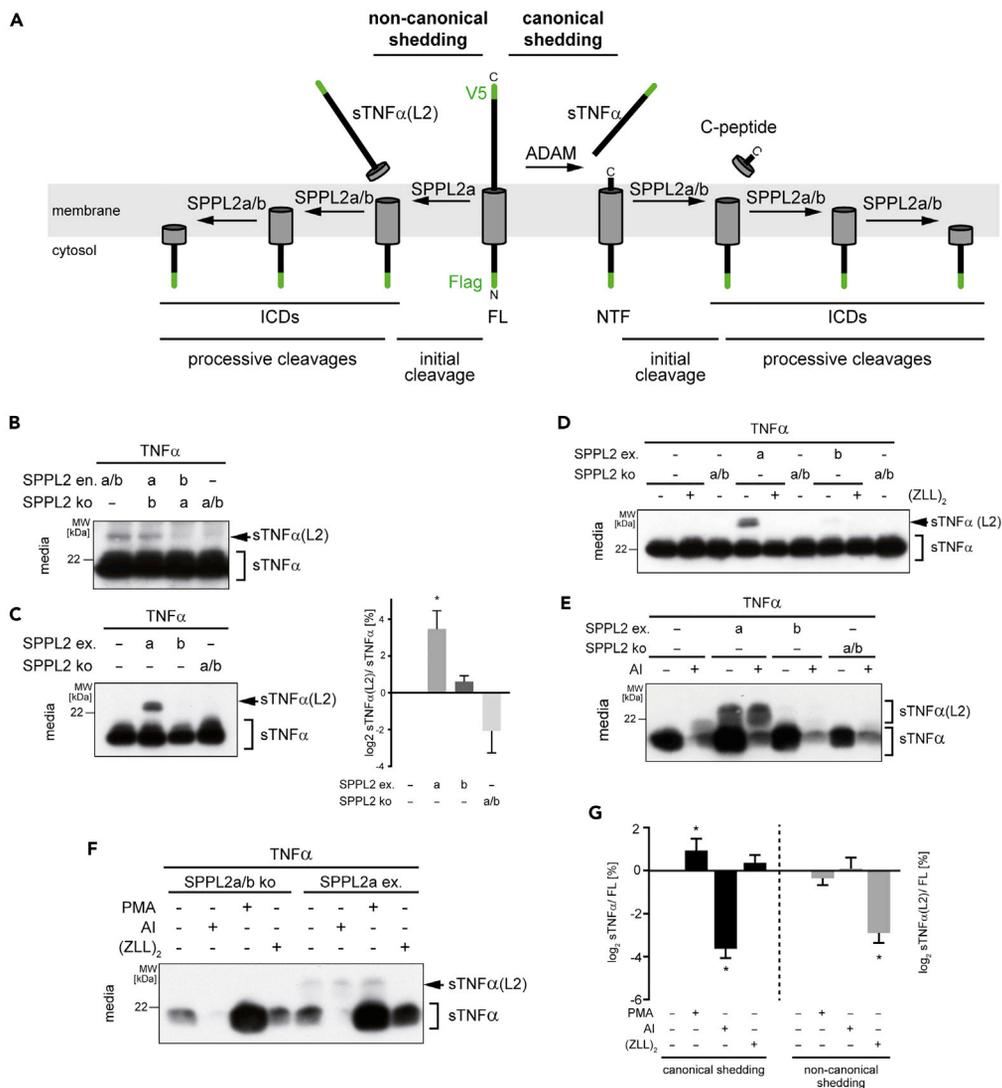
Figure 1. SPPL2a Cleaves Full-Length TNFα Independent of ADAM10/17-Mediated Shedding

(A) Schematic representation of TNFα processing. Full-length (FL) TNFα is shedded by ADAM10/17 (canonical shedding). The remaining N-terminal fragment (NTF) is sequentially cleaved by SPPL2a or SPPL2b producing several intracellular domains (ICDs) and a secreted peptide (C-peptide). In addition, SPPL2a cleaves TNFα FL directly before continuing with the processive cleavage (non-canonical shedding).

(B) Non-canonical TNFα shedding by endogenous SPPL2a. TNFα ectodomains (ECs) were immunoprecipitated from conditioned media of the HEK293 cell lines expressing endogenous (en.) levels of SPPL2a, SPPL2b, both or none (ko) and visualized utilizing the C-terminal V5-tag. sTNFα(L2), TNFα EC secreted by SPPL2 mediated shedding; sTNFα, TNFα EC secreted by ADAM mediated shedding.

(C) Ectopic SPPL2a expression (SPPL2a ex.) significantly increases sTNFα(L2) secretion. TNFα ECs were directly analyzed from conditioned media. sTNFα(L2) was quantified relative to sTNFα from respective Western blots by densitometric analysis and normalized to untreated controls, n = 3. Data are represented as mean ± SD. Statistical significance was calculated applying an unpaired, two-sided Student's t test. *p < 0.05. The Western blot shows one representative experiment.

(D) sTNFα(L2) secretion is blocked by an SPP/SPPL-specific inhibitor. TNFα ECs from conditioned media of the indicated HEK 293 cell lines were isolated and detected as in (C). Cells were treated with either 50μM Z-LL$_2$-ketone (+(ZLL)$_2$) to inhibit SPPL2 catalytic activity or with DMSO as a control (-(ZLL)$_2$).

(E) sTNFα(L2) secretion is not affected by ADAM-specific inhibitors. TNFα ECs from conditioned media of the indicated HEK 293 cell lines were isolated and detected as in (C). Cells were treated with either 5μM GI 254023X and 1μM BMS-561395 (+AI) to inhibit ADAM proteases or with DMSO as a control (-AI).

Figure 1. *Continued*

(F) Increased secretion of sTNFα does not affect sTNFα(L2) secretion. TNFα ECs from conditioned media of the indicated HEK 293 cell lines were isolated and detected as in (C). Cells were treated with either 1µM phorbol 12-myristate 13-acetate (PMA), 50µM (ZLL)$_2$, 5µM GI 254023X, and 1µM 561395 (AI) or DMSO as control.

(G) Quantification of (F). sTNFα(L2) was quantified relative to intracellular TNFα FL by densitometric analysis from Western blots as depicted in (F) and normalized to untreated controls; n = 3. Data are represented as mean ± SD. Statistical significance was calculated applying a two-way ANOVA. *p < 0.05.

whether SPPL2 proteases in addition also accept TNFα FL as a substrate, TNFα was ectopically expressed in T-Rex-293 (HEK293) cells. As expected, a prominent sTNFα fragment that is released by ADAM10/17 into the conditioned media was detected (Figure 1B). However, in addition, a slightly larger TNFα fragment (sTNFα(L2)) was secreted (Figure 1B). To evaluate whether this fragment results from cleavage by SPPL2a/b, we generated HEK293 cells that either only express endogenous SPPL2b or SPPL2a or lack both proteases using CRISPR/Cas9 (Figure S1A and S1B). Cells that only express endogenous SPPL2a still secreted sTNFα(L2), comparable to cells that express both proteases, while the protein fragment was absent in conditioned media of cells that only express SPPL2b or none of the two proteases (Figure 1B). To further support sTNFα(L2) generation by SPPL2a and to exclude that its production by SPPL2b was not only missed due to low endogenous SPPL2b expression, we ectopically co-expressed TNFα and either SPPL2a or SPPL2b and analyzed the conditioned media (Figure 1C). Ectopic expression of SPPL2a significantly enhanced sTNFα(L2) secretion compared to control cells (Figure 1C). In contrast, ectopic expression of SPPL2b did not significantly change sTNFα(L2) secretion (Figure 1C). This indicates that sTNFα(L2) is generated by SPPL2a mediated non-canonical shedding, while SPPL2b even under over-expression conditions is hardly capable of non-canonical TNFα shedding.

Treatment of cells with 2,2′-(2-Oxo-1,3-propanediyl)bis[N-[(phenylmethoxy)carbonyl]-L-leucyl-L-leucin-amide ((Z-LL)$_2$-ketone), an SPP/SPPL-specific inhibitor, significantly reduced generation of sTNFα(L2), while sTNFα secretion was not changed significantly (Figures 1D and 1G). In contrast, treatment of these cells with an ADAM10/17-specific inhibitor (AI) resulted in a significant reduction of sTNFα, while sTNFα(L2) remained unchanged compared to the respective non-treated cells (Figures 1E and 1G). Treatment with phorbol 12-myristate 13-acetate, which stimulates canonical shedding by ADAM proteases, as expected, specifically increased sTNFα, but not sTNFα(L2), release (Figures 1F and 1G), indicating that sTNFα(L2) secretion is independent of sTNFα secretion, suggesting that ADAM10/17 and SPPL2a are not competing for cleavage of TNFα wildtype (wt).

Non-Canonical TNFα Shedding Occurs at Similar Cleavage Sites as Intramembrane Cleavage

Since it is not known whether SPPL2a intramembrane cleavage in the context of RIP follows the same principles as SPPL2b intramembrane cleavage, we analyzed SPPL2a-mediated TNFα cleavage in comparison to its processing by SPPL2b.

To allow monitoring of all intramembrane cleavage products, different TNFα variants were used (Figure 2A). To visualize secreted TNFα C-peptides and thus the initial SPPL2 cleavage, a C-terminally V5-tagged TNFα variant, lacking the EC (TNFα NTF), was used. Co-expression of the TNFα NTF and SPPL2b resulted in secretion of TNFα C-peptides that were absent in cells lacking endogenous SPPL2 expression (Figure 2B). SPPL2a acted similarly and triggered the secretion of comparable TNFα C-peptide amounts (Figure 2B), suggesting that the initial endoproteolytic processing step after canonical shedding occurs with similar efficiency by both proteases. To monitor TNFα ICD production, N-terminally Flag-tagged TNFα FL was co-expressed with either SPPL2a or SPPL2b. As demonstrated before, SPPL2b co-expression resulted in efficient generation of a TNFα ICD that goes along with reduction of the TNFα NTF (Figure 2C) (Fluhrer et al., 2006, 2008). Similarly, co-expression of TNFα FL and SPPL2a resulted in conversion of TNFα NTF into TNFα ICD, while upon expression of TNFα FL in SPPL2a/b double knock-out cells, no TNFα ICD species were detected (Figure 2C). To address whether SPPL2a similar to SPPL2b utilizes processive cleavages within the TM domain to release TNFα ICD species, we performed *in vitro* conversion assays as described earlier (Fluhrer et al., 2008). Membrane preparations from cells co-expressing either SPPL2a or SPPL2b and TNFα FL were incubated at 37°C for different time intervals. Similar to SPPL2b, SPPL2a evinced processive activity, converting longer TNFα ICD species into shorter ones (Figure 2D). Using matrix-assisted laser desorption/ionisation – time of flight (MADLI-TOF) mass spectrometry, we determined whether cleavage sites of both SPPL2 proteases in TNFα are similar. Mass spectrometry of TNFα ICDs produced by SPPL2b from cleavage of TNFα FL confirmed the cleavage sites after amino acids S34 and L39 in the TM domain and
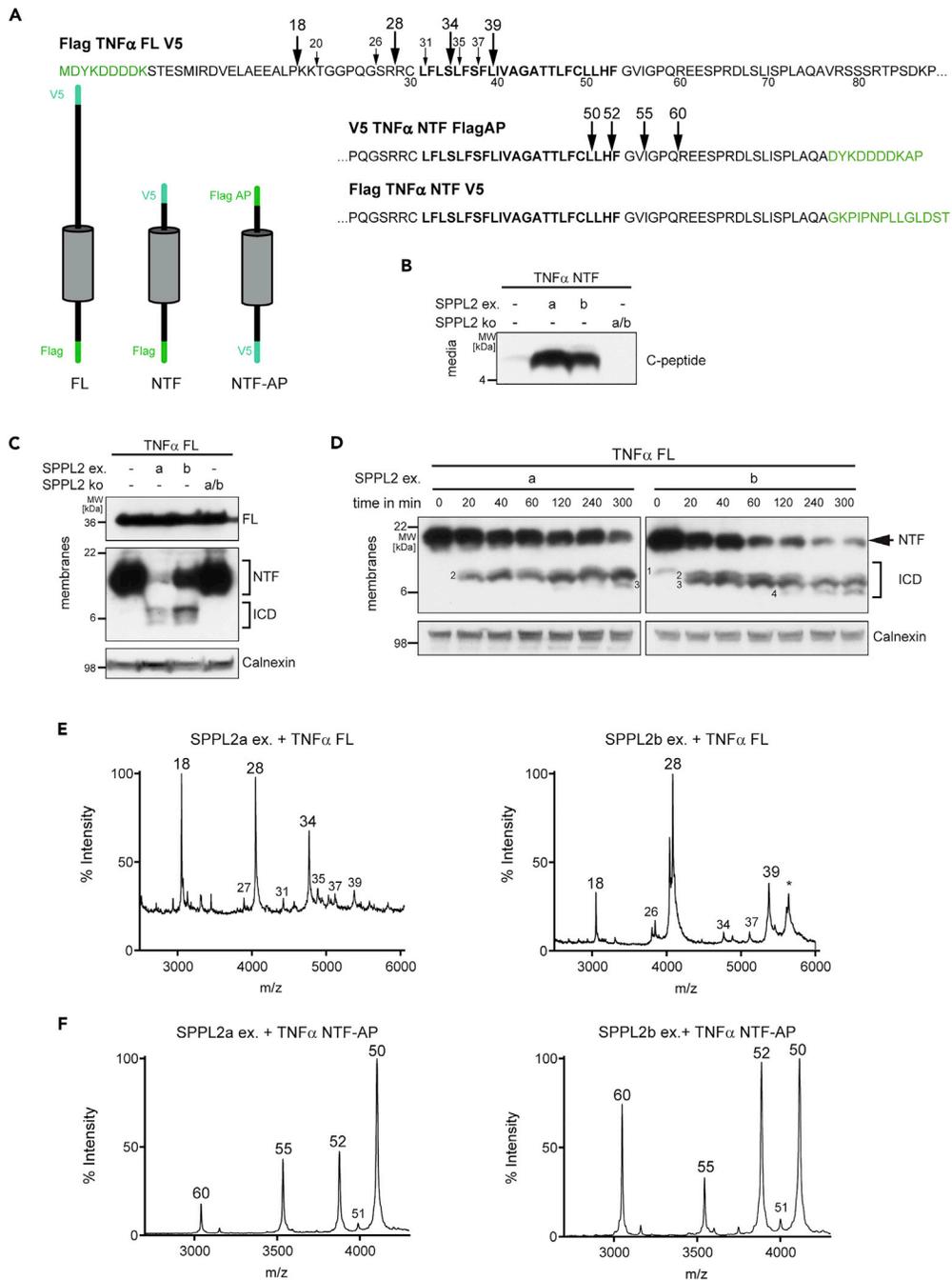
Figure 2. Processing of TNFα by SPPL2a Compared to SPPL2b

(A) Amino acid sequences and schematic representation of all TNFα variants used. Arrows indicate the peptides detected by mass spectrometry in (E).

(B) C-peptide secretion in SPPL2-expressing cells. C-peptides were immunoprecipitated from conditioned media of HEK293 cell lines expressing exogenous (ex.) levels of SPPL2a, SPPL2b, or none of the proteases (ko) and ectopically expressing the TNFα NTF using the polyclonal V5 antibody. For visualization on Western blot, the monoclonal V5 antibody was employed.

(C) ICD generation in SPPL2-expressing cells. Membranes of the indicated HEK293 cell lines ectopically expressing TNFα FL were isolated. Visualization of intracellular TNFα species was done by the monoclonal Flag antibody. Calnexin served as a loading control.

Figure 2. *Continued*

(D) Processive turnover of TNFα by SPPL2 proteases. Membranes of HEK293 cell lines co-expressing either SPPL2a or SPPL2b and TNFα FL were incubated for the indicated time periods. ICD conversion was monitored using Western blot and the Flag M2 antibody for detection. Calnexin served as a loading control.

(E) N-terminal SPPL2 cleavage sites in TNFα. Mass spectrometric analysis of ICDs generated from SPPL2a or SPPL2b, respectively. Numbers indicate the position of the most C-terminal amino acid of the respective cleavage product. * marks background peak also present in control (see Figure S2).

(F) C-terminal SPPL2 cleavage sites in TNFα. Mass spectrometric analysis of C-peptides generated from SPPL2a or SPPL2b, respectively. Numbers indicate the position of the most N-terminal amino acid of the respective cleavage product.

the release of additional smaller peptides ranging from 18 to 28 amino acids in length as reported before (Figures 2E and S2) (Fluhrer et al., 2006). In addition to our earlier study, we now, due to increased sensitivity of the mass spectrometry analysis, identified an additional consecutive cleavage site at Ser37 (Figure 2E). TNFα ICDs released by SPPL2a were qualitatively similar (Figure 2E), but cleavage after S34 occurred more efficiently in SPPL2a-expressing cells compared to SPPL2b-expressing cells. In contrast, cleavage after L39 was the dominant intramembrane cleavage product in SPPL2b-expressing cells (Figure 2E). To allow mass spectrometric detection of TNFα C-peptides, we used a TNFα NTF version that carries a Flag-tag stabilized by alanine and proline at the C-terminus (TNFα NTF-AP; Figure 2A). Analysis of TNFα C-peptides released by SPPL2b confirmed the two major cleavage sites at L50 and H52 (Figures 2F and S2) (Fluhrer et al., 2006). Additionally, two smaller C-peptides resulting from cleavages at V55 and R60 were identified (Figures 2F and S2). Both C-peptide species were not detected in our initial study (Fluhrer et al., 2006) since they do not contain any of the amino acids that were used to label the cleavage products radioactively. These C-peptides emerge from cleavages in the luminal JM domain of TNFα. Although we cannot finally exclude that these shorter C-peptides originate from unrelated exopeptidases present in the conditioned media, the pattern observed suggests that SPPL2b-mediated endoproteolysis also occurs in the luminal JM domain in close vicinity to the TM domain. SPPL2a essentially secreted the same C-peptide species, although the shorter C-peptide species were less abundant (Figures 2F and S2).

Based on this, we next analyzed whether the SPPL2a non-canonical shedding that results in sTNFα(L2) secretion occurs at the same positions as the cleavages that release TNFα C-peptides in the context of RIP. To determine the N-termini of the soluble TNFα species, we established a TNFα FL version that harbors an internal Flag-tag followed by a TEV protease (isolated from Tobacco Etch Virus) cleavage site C-terminally of the amino acid that terminates TNFα NTF (TNFα FlagTEV; Figure 3A). Processing of TNFα FlagTEV by SPPL2a essentially resembled that of TNFα wt (Figure 3B), and transport of TNFα FlagTEV to the cell surface occurred with similar efficiency as that of TNFα wt (Figure S3A). To analyze the cleavage sites of SPPL2a in TNFα FlagTEV, cleavage products were isolated from conditioned media by immunopre-cipitation utilizing the Flag-tag. The isolated protein fragments were subjected to TEV-protease cleavage; peptide fragments containing a Flag-tag were again immunoprecipitated and subjected to MALDI-TOF mass spectrometry. The analysis revealed two groups of peptides, one reflecting cleavages at the known SPPL2 sites (Fluhrer et al., 2006, Figure 2F) and the other comprising much smaller peptides that match the known ADAM10/17 cleavage sites (Figures 3C, S3B, and S3C) (Mohan et al., 2002). To ensure that the group of larger peptides was indeed generated by SPPL2a cleavage, cells were treated with the SPP/SPPL inhib-itor (Z-LL)$_2$-ketone prior to analysis. As expected, secretion of all peptides ranging from 4 to 6 kDa was strongly reduced, while secretion of peptides resulting from ADAM10/17 cleavage remained unchanged (Figure 3D). Thus, we conclude that SPPL2a non-canonical shedding occurs at the same cleavage sites as cleavage of TNFα by SPPL2a in the context of RIP. Interestingly, however, the most dominant cleavage site of SPPL2a non-canonical shedding mapped to cleavage at V55, while the dominant cleavage sites of intramembrane cleavage were detected at L50 and H52 (Figure 2F).

The Primary Structure of the TNFα TM Domain Affects Non-Canonical Shedding

Earlier studies suggested that intramembrane proteolysis by GxGD-aspartyl proteases is affected by the conformational flexibility of a substrate's TM helix (Fluhrer et al., 2012; Götz et al., 2019b; Langosch et al., 2015; Langosch and Steiner, 2017). To elucidate whether similar determinants also influence SPPL2a-mediated non-canonical shedding of TNFα, all serines (S34, S37), glycines (G43), cysteine (C49), and histidines (H52) in the TNFα TM domain were substituted by alanine, leucine, or proline. While glycine residues facilitate local helix bending and change its collective dynamics (Högel et al., 2018), polar residues form stabilizing hydrogen bonds that potentially form between their side chains and the main-chain
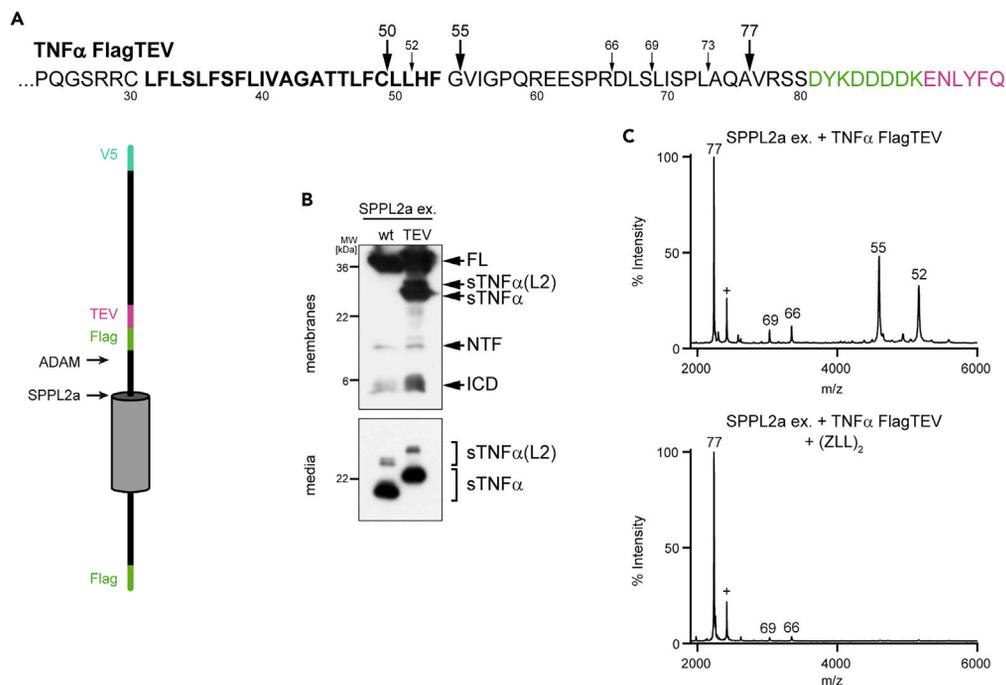
Figure 3. Cleavage Sites of SPPL2a-Mediated Non-Canonical TNFα Shedding

(A) Amino acid sequence and schematic representation of TNFα FlagTEV. Arrows indicate the cleavage sites of the respective proteases.

(B) Processing of TNFα wt and TNFα FlagTEV is essentially similar. Membranes of HEK 293 cells co-expressing SPPL2a (SPPL2a ex.) and the indicated TNFα variant were analyzed on Western blot using the monoclonal Flag M2 antibody to detect all intracellular TNFα fragments. The respective conditioned media were visualized with the monoclonal V5 antibody to detect secreted TNFα EC variants.

(C and D) Cleavage sites of the secreted TNFα ectodomain variants. Secreted EC from HEK 293 cells co-expressing SPPL2a and TNFα FlagTEV were treated with 50μM (ZLL)$_2$ (D) or DMSO (C). Numbers indicate the position of the most N-terminal amino acid of the respective cleavage product. Peaks from 66 to 77 reflect cleavage of TNFα by ADAM proteases. Peaks from 50 to 55 reflect cleavage of TNFα by SPPL2a. + marks peak of unknown identity

carbonyl oxygens of upstream residues (Gray and Matthews, 1984; Scharnagl et al., 2014). Alanine or leucine can rigidify a TM helix by non-polar interactions of its flexible side chain with neighboring residues, whereby the effect of leucine on helix stabilization is supposed to be stronger than that of alanine (Quint et al., 2010). In contrast, proline destabilizes TM helices, as it cannot form an amide hydrogen bond and its cyclic side chain clashes with its N-terminal neighbor (Cordes et al., 2002).

All TNFα mutants were co-expressed at similar amounts with SPPL2a in HEK293 cells (Figure 4A). Substitutions of S34, S37, G43, and C49 by proline significantly enhanced SPPL2a-dependent non-canonical TNFα shedding, while an H52P mutation had no effect (Figures 4A and 4B). In contrast, leucine substitutions at all positions decreased non-canonical SPPL2a shedding, with C49L and H52L having the strongest effect (Figures 4A and 4B). Alanine substitutions at all positions had only minor impact on non-canonical shedding.

Similar to the G37/G38 hinge of the APP TM helix (Götz et al., 2019b), G43 may increase helix flexibility at the center of the TNFα TM domain. Interestingly, an even stronger helix destabilization at this position by the G43P mutation caused the most pronounced increase in non-canonical shedding. In contrast, the attempt to stabilize this site by the G43L mutation had only a very minor effect. Since the destabilizing function of glycine results from a packing defect due to its missing side chain (Högel et al., 2018), we reasoned that the small side chain of both neighboring alanine residues might also contribute to local helix flexibility. This compares to the sequence context of the G37G38 hinge of the C99 TM helix, where the GG motif is flanked by insufficiently packing VAL residues V36, V39, V40 (Götz et al., 2019b; Hitzenberger et al., 2020). Consequently, we replaced the A$_{42}$G$_{43}$A$_{44}$ motif by leucine residues (TNFα AGA/LLL). Indeed, this resulted in an almost complete loss of SPPL2a-mediated non-canonical shedding (Figures 4C and 4D).
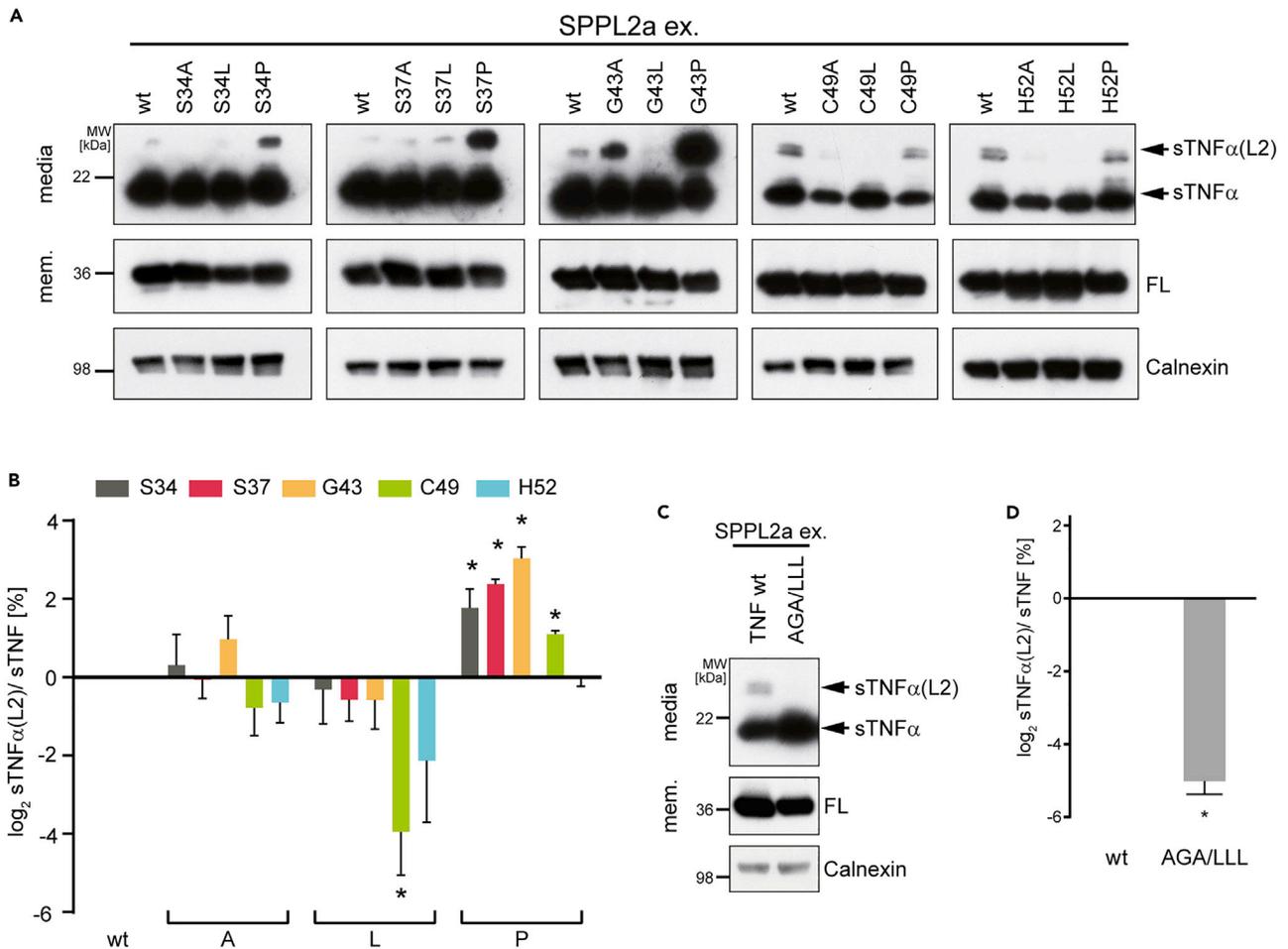
Figure 4. Modulating Non-Canonical Shedding by Mutations in the TM Domain

(A) Mutations in the TM domain of TNFα affect non-canonical shedding by SPPL2a. Secreted TNFα from media of cells co-expressing SPPL2a (SPPL2a ex.), and the respective TNFα mutant was analyzed using the V5 antibody. Detection of TNFα FL from membranes served as a transfection control and calnexin as a loading control.

(B) Quantification of (A). sTNFα(L2) was quantified relative to sTNFα from respective Western blots by densiometric analysis and normalized to TNFα wt, n = 3. Data are represented as mean $\pm$ SD. Statistical significance was calculated applying an unpaired two-sided Student's t-test. *p < 0,05.

(C) Insertion of a triple L motif reduces SPPL2a shedding. sTNFα from TNFα wt and the AGA/LLL variant was detected with the V5 antibody in media of cells co-expressing SPPL2a.

(D) Quantification of (C). sTNFα(L2) was quantified relative to sTNFα from respective Western blots by densiometric analysis and normalized to TNFα wt, n = 3. Data represented as mean $\pm$ SD. Statistical significance was calculated applying an unpaired Student's t-test. *p = 0,01.

Although SPPL2b does not act as a non-canonical sheddase on TNFα wt (Figure 1), proline substitutions at positions S34, S37, as well as G43, allowed non-canonical shedding also by SPPL2b (Figure S4).

These data demonstrate that proline mutations that disturb helical geometry of TM domains support non-canonical shedding of TNFα, while leucine mutations tend to have the opposite effect. Interestingly, leucine substitutions had the strongest impact in the C-terminal part of the TM domain, while the increase of non-canonical shedding by proline substitutions in the N-terminal half was most pronounced.

Mutations Affecting the Efficiency of TNFα Cleavage by SPPL2a Do Not Alter the Cleavage Sites

To elucidate whether increased non-canonical shedding induced by proline substitutions also affected the SPPL2a cleavage sites, we performed mass spectrometric analysis of the respective TNFα C-peptides. Pro-line substitutions that significantly increased non-canonical shedding of SPPL2a (S34P, S37P, G43P, and C49P) did not change SPPL2a cleavage sites (Figure 5). Interestingly, H52P, which had no effect on cleavage
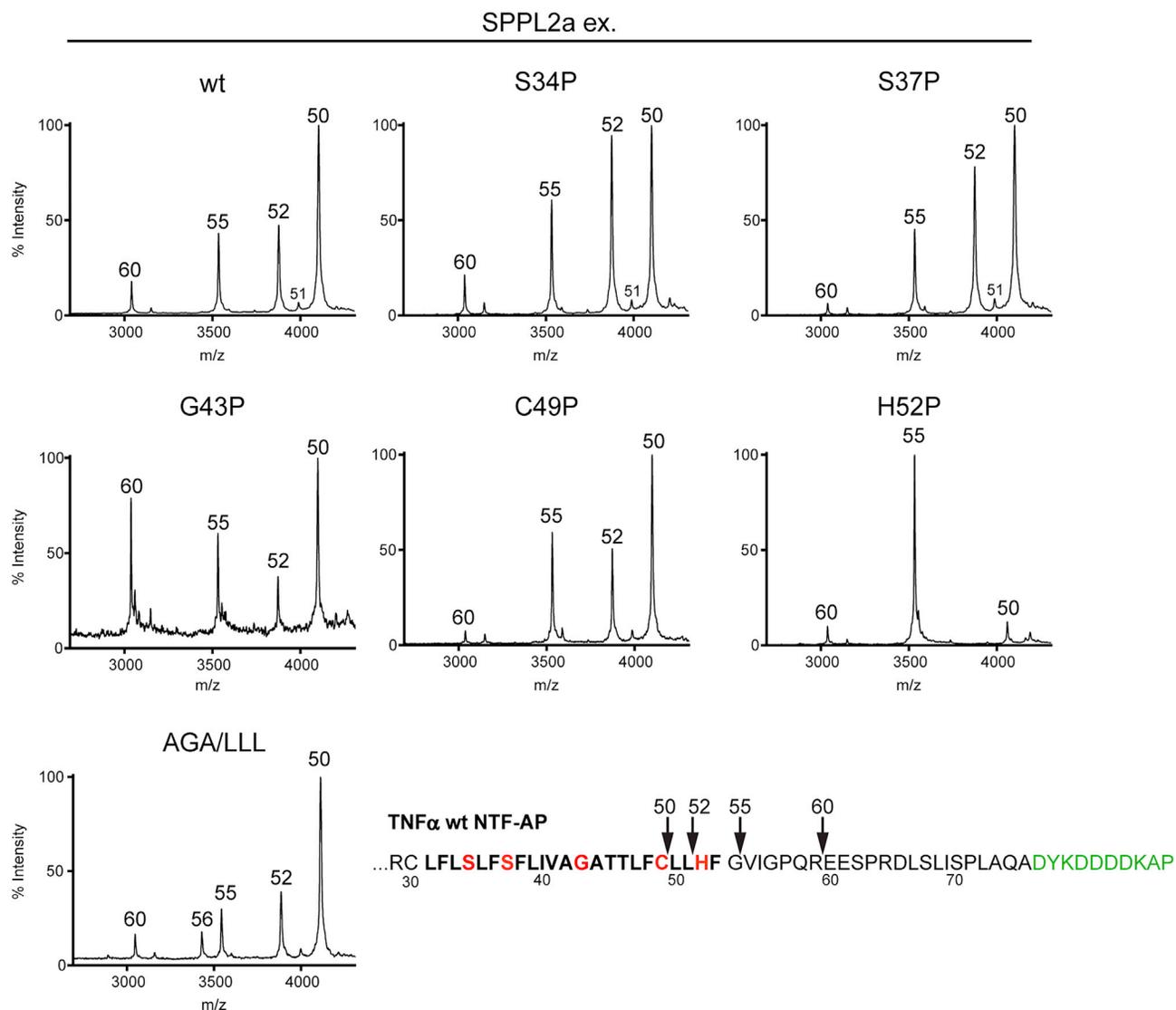
Figure 5. Cleavage Sites of SPPL2a in TNFα Mutants Are Not Changed
Secreted C-peptide was immunoprecipitated from media of HEK293 cells co-expressing SPPL2a with anti-Flag M2 affinity gel and analyzed via mass spectrometry. Numbers indicate the position of the most N-terminal amino acid of the respective cleavage product.

efficiency, resulted in an almost complete loss of the major cleavages sites at leucine 50 and histidine 52, and cleavage at V55 became the major cleavage product (Figure 5). In contrast, C49P, which also changes an amino acid directly at one of the major cleavage sites, did not result in loss of a specific cleavage product (Figure 5). While proline substitutions at S34 and S37 relatively increased cleavage at H52, the proline substitution at G43 relatively increased cleavage at R60 (Figure 5).

These data indicate that initial cleavage of SPPL2a at H52 is more dependent on certain primary sequence requirements than, for instance, cleavage at C49, and disruption of the α-helix at H52 seems not to be tolerated by SPPL2a. In addition, proline substitutions in the N-terminal half of the TNFα TM domain affected the preferred position of the initial cleavage at the C-terminal membrane border, pointing to distance effects of these mutations.

Since proline substitutions increased non-canonical TNFα shedding to levels comparable with the physiologically very important canonical shedding (Figures 4A and 4B) (Brenner et al., 2015; So and Ishii, 2019), it is tempting to speculate that further substrates that are efficiently shed by SPPL2a exist. To provide the basis

to identify such substrates, e.g., by use of tailored prediction algorithms, we aimed to characterize the dynamical and structural changes induced by these mutations using deuterium/hydrogen exchange (DHX), NMR spectroscopy, and molecular dynamic (MD) simulations.

Deuterium/Hydrogen Exchange Suggests a Central Flexible Region in the TNFα wt TM Helix

Using DHX kinetics, we investigated selected mutants that drastically affected the efficiency of non-canonical shedding by SPPL2a and were designed to change the conformational flexibility of the TNFα TM helix. Specifically, we compared TNFα wt to S34P, the most N-terminal mutation that significantly increased initial cleavage at the C-terminal end, and to S34A, which did not affect non-canonical shedding, as well as to AGA/LLL, which significantly reduced SPPL2a non-canonical shedding. DHX was recorded on corresponding synthetic peptides that included the complete predicted TNFα TM domain and parts of the JM domains (Figure S5A), including naturally occurring basic residues that improve solubility of the peptides. As done previously (Pester et al., 2013), DHX kinetics of exhaustively (>95%) deuterated peptides were measured at 20°C and pH 5 in 80% (v/v) trifluoroethanol (TFE), a solvent that supports helicity and the low content of water mimics the aqueous environment near the catalytic residues of aspartate intramembrane proteases (Sato et al., 2006). In contrast to membrane-embedded peptides, TFE allows effective exchange from hydrophobic residues (Poschner et al., 2009).

First, we examined the overall DHX kinetics of the peptides. At the start, when labile deuterons bound to polar or non-H-bonded heavy atoms have already exchanged to protons, ∼25 amide deuterons remain, i.e. ∼90% of those 28 backbone amides that can be partially protected from DHX by intrahelical H-bond formation (Figure S5B). Over time, isotope patterns gradually shifted and the isotopic distributions lacked a bimodal shape (data not shown). This behavior is diagnostic of EX2 kinetics where individual deuterons are exchanged in an uncorrelated fashion, thus indicating transient local helix unfolding events (Konermann et al., 2011; Xiao et al., 2005). The overall exchange kinetics of TNFα wt and S34A peptides were similar, while the exchange rate in S34P was higher and it was strongly reduced in AGA/LLL (Figure S5B). In the second step, we employed gas-phase fragmentation by electron transfer dissociation after different periods of DHX in order to resolve amide H-bond strength of the helices at the single-residue level. From the DHX kinetics of the fragment ions, we determined the residue-specific free energy changes ΔG associated with the disruption of amide H-bonds (Figure 6A) based on the amide exchange rate constants k_{exp} (Figure S5B and Table S1) (Yucel et al., 2019). Some amides (T46, L50) are described only insufficiently due to poor fragmentation efficiencies and/or overlap of isobaric fragments.

The ΔG values obtained for the TNFα wt TM helix range from ∼1 kcal/mol to ∼4.5 kcal/mol. Values of ∼1 kcal/mol were previously reported for intrahelical H-bonds in water, which are weak since intrahelical H-bonding competes with helix-water H-bonding, ∼4 kcal/mol for H-bonds of model compounds in apolar solvent, and 6.6 kcal/mol for H-bonds in vacuo (Bowie, 2011). In the standard amide H-bonding pattern of an α-helix, the nitrogen of a residue at position (i) forms H-bonds to the carbonyl oxygens at residues (i-3) and (i-4). Thus, in the TNFα helix, nitrogens of T45, L47, and F48 form H-bonds with V41/A42, G43/A44, and A44/T45 carbonyls, respectively. Interestingly, their stabilities are ∼1 kcal/mol below those of their neighbors. This is consistent with the existence of a flexible region from V41 to T45 (Stelzer and Langosch, 2019). Glycine and, by analogy, alanine induce a local packing defect which can facilitate helix bending (Högel et al., 2018), which in turn destabilizes H-bonding to upstream (i,i+3,4) amides, as observed here. The L47/F48 carbonyls also formed low stability (i+3,4) H-bonds with L51. Only minor differences in H-bond strength in the N-terminal region were observed between the amides of TNFα wt and the S34A mutant (Figure 6B). In contrast, the S34P mutation markedly weakened H-bonds in that region, in particular between F36 and L39 (Figure 6B). ΔG values around position 34 could not be determined as exchange is too rapid for experimental resolution close to the frayed helix termini. Importantly, compared to TNFα wt, the AGA/LLL mutant exhibited a markedly enhanced H-bond strength ranging from I40 up to the initial cleavage site of SPPL2a at C49, which effectively compensates the reductions of H-bond stability seen with the wt (Figure 6B).

In summary, these data indicate the presence of a flexible region in the center of the TNFα wt TM domain that may reflect a potential hinge region, similar to that observed in the APP TM domain (Barrett et al., 2012; Götz et al., 2019b). S34P induces a significant destabilization in the N-terminal part of the TNFα TM helix up to the potential hinge region. In contrast, the AGA/LLL mutation resulted in a marked stabilization in the center of the TM helix. However, these data do not explain the distance effect of S34P on the C-terminal cleavage site that was observed in the cellular cleavage assays.
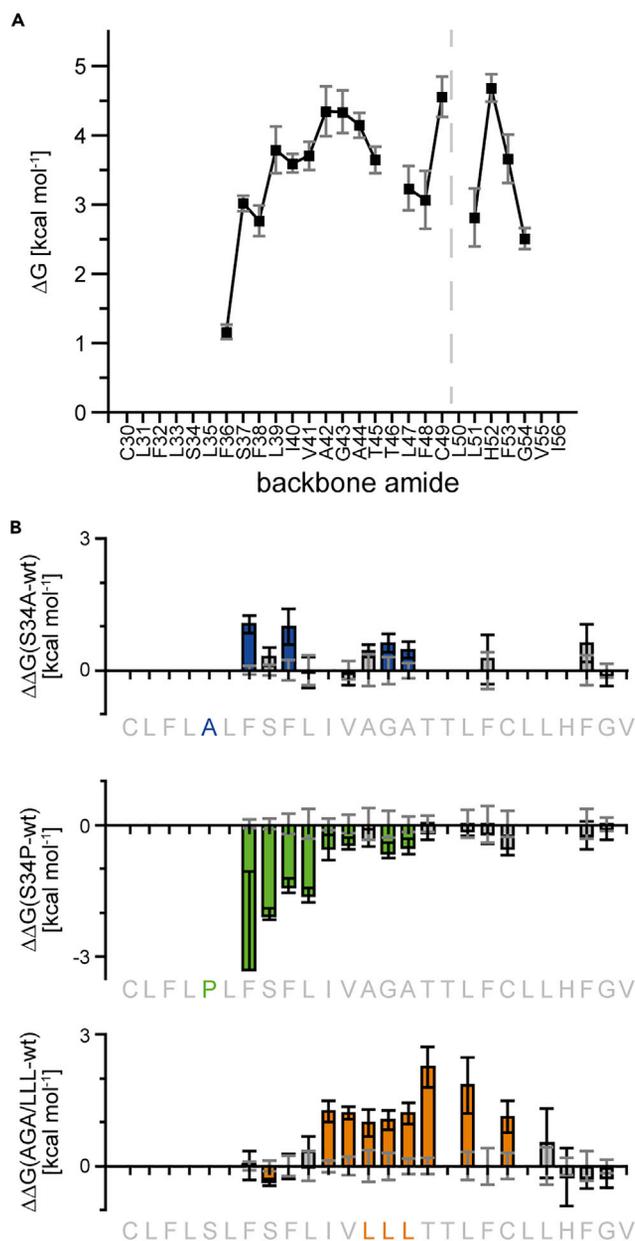
Figure 6. Analysis of TNFα TM Helix Flexibility by DHX

(A) Calculated Gibb's free energy differences ΔG of amide H-bond disruption of the TNFα wt TM helix. Error bars correspond to standard confidence intervals (calculated from the errors of fit in k_{exp} determination). Broken lines denote the major initial SPPL2a cleavage sites.

(B) Differences ΔΔG between TNFα mutant and wt amides (± confidence intervals of mutants). Confidence intervals of wt amides are plotted in light gray on the x axis. In the case of the colored bars, the confidence intervals of mutant and wt are not overlapping while they do overlap in the case of the gray bars.

NMR Spectroscopy Reveals the Structure of the TNFα TM Helix and the Impact of Mutations on a Central Bend

To further interpret the data obtained from DHX kinetics and to unravel the distance effect on the C-terminal cleavage site, we determined the 3D structures of TNFα wt, the S34P, and the AGA/LLL mutant TM domain peptides (Figure 7A) in TFE:H$_2$O (80:20, v:v) by NMR spectroscopy. Amino acids which take part in an α-helical conformation show short-range cross peaks between amide protons (dNN(i, i+1)), Hα and amide protons (dαN(i, i+3)), as well as Hα and Hβ protons (dαβ(i, i+3)) in ^{1}H^{1}H-NOESY spectra
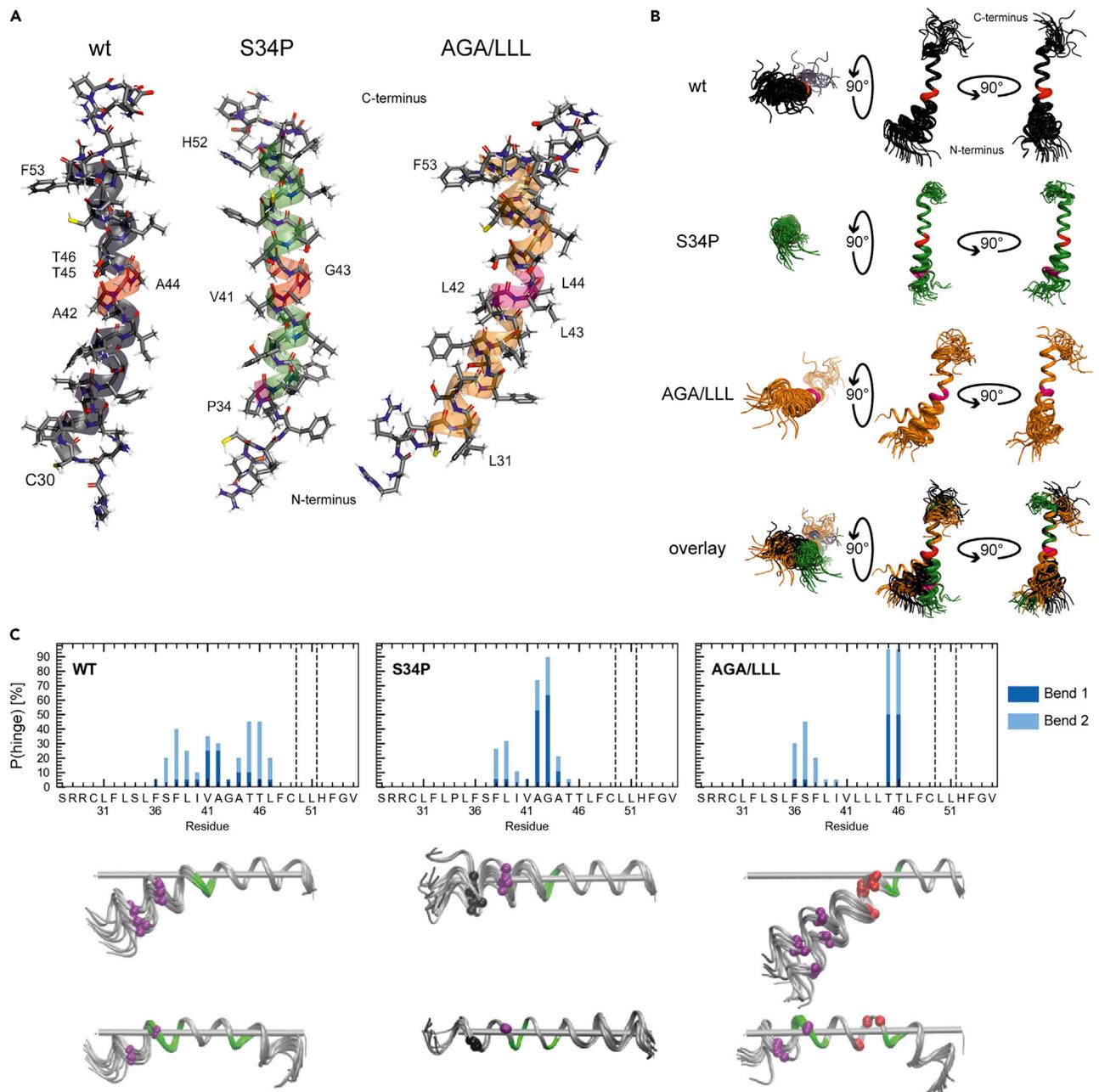
Figure 7. 3D Structural Analysis of the TNFα TM Segment by NMR

(A) Solution structures of TNFα wt (black), TNFα S34P (green), and TNFα AGALLL (orange). The A42/G43/A44 motif is represented in red (wt and S34P), respectively, in pink in AGA/LLL. P34 in S34P is shown in pink.

(B) Structural bundles of TNFα wt (black), TNFα S34P (green), and TNFα AGA/LLL (orange). Top and side views of the 20 best structures superimposed onto the backbone of C-terminal helix from residue 42 to 53. The A42/G43/A44 motif is represented in red. Amino acid exchanges in the respective mutants are highlighted in magenta.

(C) Backbone conformations of NMR structures. Top section: Probability that a residue is part of a single hinge (type Bend 1) or a pair of hinges (type Bend 2). Dashed lines indicate cleavage sites. Bottom section: Bend 1 and Bend 2 subsets aligned to an ideal reference helix (gray cylinder). The hinges (green) are coordinating bending between helical segments. Bend 1 structures were aligned to the helical C-terminal segment of the reference structure (gray cylinder); Bend 2 conformations were aligned to the helical segment between the two hinges. The location of S34 and S37 Cα atoms is highlighted as purple spheres. Mutation sites are drawn in space fill mode (Leu: red, Pro: black). Exemplary conformations illustrating the fundamental motions are explained in more detail in (Götz et al., 2019b; Götz and Scharnagl, 2018).

(Figure S6A) (Wüthrich, 1986). Further, deviations of chemical shifts from random coil values, denoted as secondary chemical shifts $\Delta\delta$, are sensitive to protein secondary structure, with helical conformation resulting in positive secondary shifts of $^{13}C\alpha$ (Wishart et al., 1991) and negative secondary shifts of $^{1}H\alpha$, as well as $^{13}C\beta$ (Spera and Bax, 1991; Wishart et al., 1991).

In the TNFα wt peptide, the pattern of dNN(i, i+1), dαN(i, i+3), and especially d$\alpha\beta$(i, i+3) NOE peaks, as well as secondary chemical shifts, indicated a helical segment ranging from residue C30 to F53 (Figure S6). The 3D structure revealed a slight bend in the center of the helix at the A42/G43/A44 motif (Figure 7A). In this region, secondary chemical shifts and the number of characteristic d$\alpha\beta$(i, i+3) NOE peaks were reduced, supporting a disturbance of the α-helix (Figure S6). Furthermore, the presence of dαN(i, i+2) NOEs in this region is indicative for a 3$_{10}$-helix contribution. The 3$_{10}$-helix has been proposed as an intermediate in folding and unfolding of α-helices and therefore suggests a disruption of a regular α-helix (Millhauser, 1995; Wüthrich, 1986). The N-terminus of the α-helix, and in particular its first turn (L31 to L35), showed a lower number of d$\alpha\beta$(i, i+3) NOEs and less pronounced secondary chemical shifts, while the C-terminal helical part (T45 to F53) formed a more stable α-helix reflected by a regular pattern of characteristic NOEs and higher secondary chemical shifts (Figure S6). The side chain γ-hydroxyl proton of T45 showed a clear resonance and an NOE contact to the methyl group of V41. Since this hydroxyl proton is in H-bonding distance to the main chain carbonyls of V41 or A42, it might stabilize the α-helix at A42. This side chain/main chain H-bond might also promote the bend in the middle of the helix. The orientation of the N-terminal TM part with respect to the C-terminal part was not static, but slightly flexible, whereby the mutual orientation of the two parts was not arbitrary (Figure 7B). To visualize the flexibility of the TNFα TM domain, we superimposed the NMR models onto the backbone of the C-terminal part from A42 to F53. This revealed that the orientation of the N-terminal part with respect to the C-terminal part cannot be fully restrained. Yet, the mutual orientation of the two helical regions underlies constraints as the N-terminal helices are located within a narrow cone with A44 lying on the convex side of the bend (Figure 7B).

In the S34P mutant, the helix started N-terminally at P34 and, thus, is a full helical turn shorter than in the wt structure (Figure 7A). The region between C30 and P34 was characterized by very long amide H-bonds and a severely distorted structure as indicated by secondary chemical shifts and the NOE pattern (Figure S6). Additionally, dαN(i, i+2) NOEs and the presence of dαN(i, i+4) NOEs in the N-terminal helix (P34 to V41) may be interpreted as a mixture of random coil and α-helix, as well as a mixture of 3$_{10}$-helix and α-helix. As expected, this indicated a less stable or more distorted α-helix (Millhauser, 1995), which comprises greater flexibility compared to the TNFα wt TM domain. As in TNFα wt, the side chain γ-hydroxyl proton of T45 marks the beginning of the C-terminal part and revealed an NOE contact to the methyl group of V41. Interestingly, the bend in the center of S34P was less pronounced (Figure 7A). Consequently, the S34P mutation not only resulted in a shortened N-terminal helix but also straightened the entire TNFα TM helix. Superposition of S34P structures onto the backbone of the C-terminal part indicates that the N-terminal part lies within a smaller cone. Interestingly, they bend in a different direction in comparison to TNFα wt, and A44 now lies at the concave side and A42 on the convex side of the bend (Figure 7B).

Similar to the TNFα wt TM domain, the AGA/LLL mutant formed an α-helix from C30 to F53, but, as expected, the central region containing the leucine substitutions was more stable, as indicated by the secondary chemical shifts and NOE pattern (Figure S6). In addition to the T45 side chain γ-hydroxyl proton, that of T46 also showed an NOE contact to the methyl group of L4. This suggests that this T46 hydroxyl hydrogen forms an H-bond to the main chain carbonyls of leucines at position 42 or 43, reflecting a more stable structure of AGA/LLL in accordance with the DHX experiments. By superimposing the structures of the AGA/LLL mutant onto the backbone of the C-terminal part ranging from L42 to F53, the N-terminal part is found within a comparable cone as in TNFα wt (Figure 7B). However, the bulky leucine residues bend the helix in direction of V41/T45 (Figure 7B). This effect may especially be transmitted through the two adjacent threonines (T45, T46). Since their side chain hydroxyl groups form hydrogen bonds to the main chain (V41, A42, and A43), any change in their orientation affects the direction of the N-terminal helix.

A quantitative characterization of the NMR conformational ensembles with respect to location of mechanical hinges using the program Dyndom complements this analysis (Götz et al., 2019a, 2019b; Hayward and Lee, 2002). In this context, in order to act as hinge, a flexible region ($\geq$ 2 residues) has (i) to be flanked by more rigid helical segments, and (ii) to be part of an intact H-bond network that coordinates the motions of the flanking segments relative to each other (Götz et al., 2019a, 2019b). Generally, the N- and C-terminal

parts of helical peptides can bend and twist around a single hinge, which is referred to as Bend1 and Twist1 motions, respectively. In another conformational subset, the terminal helix segments bend or twist with respect to the helical center segment around a pair of hinges, which is referred to as Bend2 and Twist2 motions, respectively. Steric conformation of the side chain, as well as stability of H-bonds spanning the hinge and connecting it with the flanks, determines extent and direction of conformational changes.

For the TNFα wt peptide and AGA/LLL mutant, Bend1 and Bend2 conformations are equally probable, while the S34P mutants prefer single-hinge bending. Helix twisting was not observed. In the Bend1 conformations of TNFα wt, the hinge is located at V41A42 in the helix center (Figure 7C). The S34P and the AGA/LLL shift the Bend1 hinge downstream to T45/T46 or A42/G43, respectively. These residues also form part of the double hinge in Bend 2 conformations, where the second hinge is located in the N-terminal part of the helix and shifts from S37/F38/L39 in TNFα wt to F36/S37 in the AGA/LLL mutant and F38/L39 in S34P (Figure 7C). Besides the mutation-induced hinge shifts, we also observe differences with respect to the extent of bending. For TNFα wt, the mean bending angle between the helical segments is ~25° for both Bend1 and Bend2 conformations. The S34P mutation reduces bending to ~10°, while the AGA/LLL mutation allows for a ~10° larger bending. TNFα wt and the AGA/LLL mutant show the same preference for the direction of bending.

In line with the DHX experiments (Figure 6), the NMR data demonstrate that S34P destabilizes the N-terminal part of the TNFα TM helix, while the AGA/LLL mutation stabilized its central region. N- and C-terminal parts of the TNFα wt TM domain adapt a defined relative orientation to each other. Most likely, this is facilitated by a flexible, but still helical, bend in the center of the TM domain. Interestingly, the S34P mutation induced a straighter orientation of the two parts, while the AGA/LLL induced a C-terminal shift of the bend and slightly changed the extent and direction of the bend (see below). This may explain the distance effects observed in the cleavage assays (Figure 4).

MD Simulations Predict Impact of Mutations on TM Helix Tilt and C-Terminal Residue Insertion in a Membrane

In order to study TM helix dynamics in a membrane, we performed microsecond atomistic MD simulations of the TMFα wt TM helix (residues 22–62), as well as the S34A, S34P, and AGA/LLL mutants, in a fully hydrated 1-palmitoyl-2-oleoyl-sn-glycero-3-phosphocholine (POPC) bilayer.

All mutations affected the orientation of the TM helix (F36-C49) with respect to the membrane normal (Figures 8A and 8C). The S34A and S34P mutations were predicted to increase the tilt angle from an average of ~15° in the TNFα wt peptide to ~50° in the mutants, while the AGA/LLL mutation induces a second population tilting with ~35° in the simulation. An increased tilt angle goes along with an increased membrane insertion depth of residues at the C-terminal interface (Figures 8A and 8B) which would in turn stabilize the helix and increase its length as predicted by secondary structure analysis using the DSSP algorithm (Figure S7A) (Kabsch and Sander, 1983). Orientation of the TM domain, as well as location of the cleavage site, might have an impact on the initial encounter of the substrate's TM domain with the enzyme. However, neither simulated tilt angle distributions nor helix lengths show a clear correlation to the cleavage efficiencies of the respective mutants.

Next, we investigated the occupancy of intrahelical H-bonds, i.e., the probability of a backbone carboxyl at position i forming a α-H-bond or a 3_{10}-H-bond with an amide in either i+4 or i+3. For the TNFα wt and all mutants, a slightly lower occupancy of α-H-bonds emanating from L35/F36/S37 backbone carboxyl was calculated (Figure S7B), which is compensated by formation of 3_{10}-H-bonds (Figure S7C). For residues at the C-terminal membrane interface, i.e., the region of the initial SPPL2a cleavage sites, notable shifting from α- to 3_{10}-H-bonds was detected, where the onset of α-H-bond instabilities correlates with residue insertion depths. Interestingly, in the S34P mutant, the percentage of these 3_{10}-H-bonds was lower and slightly C-terminally shifted, which may produce functional TM helix flexibility (Cao and Bowie, 2012).

Finally, we applied the same method as for analysis of the NMR conformational ensembles to investigate helix flexibility in terms of hinge bending and twisting motions of the TNFα peptides in a POPC membrane bilayer. While the S34P mutation introduces a structural kink, i.e., a strong permanent bending around a hinge localized at L33/P34 in >70% of the structures, deviations from a straight helix in TNFα wt, S34A, and AGA/LLL are <30%, distributed over three helix turns and involve four different conformational classes with per-residue hinge propensities <10% (Figure 8D). Constraints imposed by the lipid environment
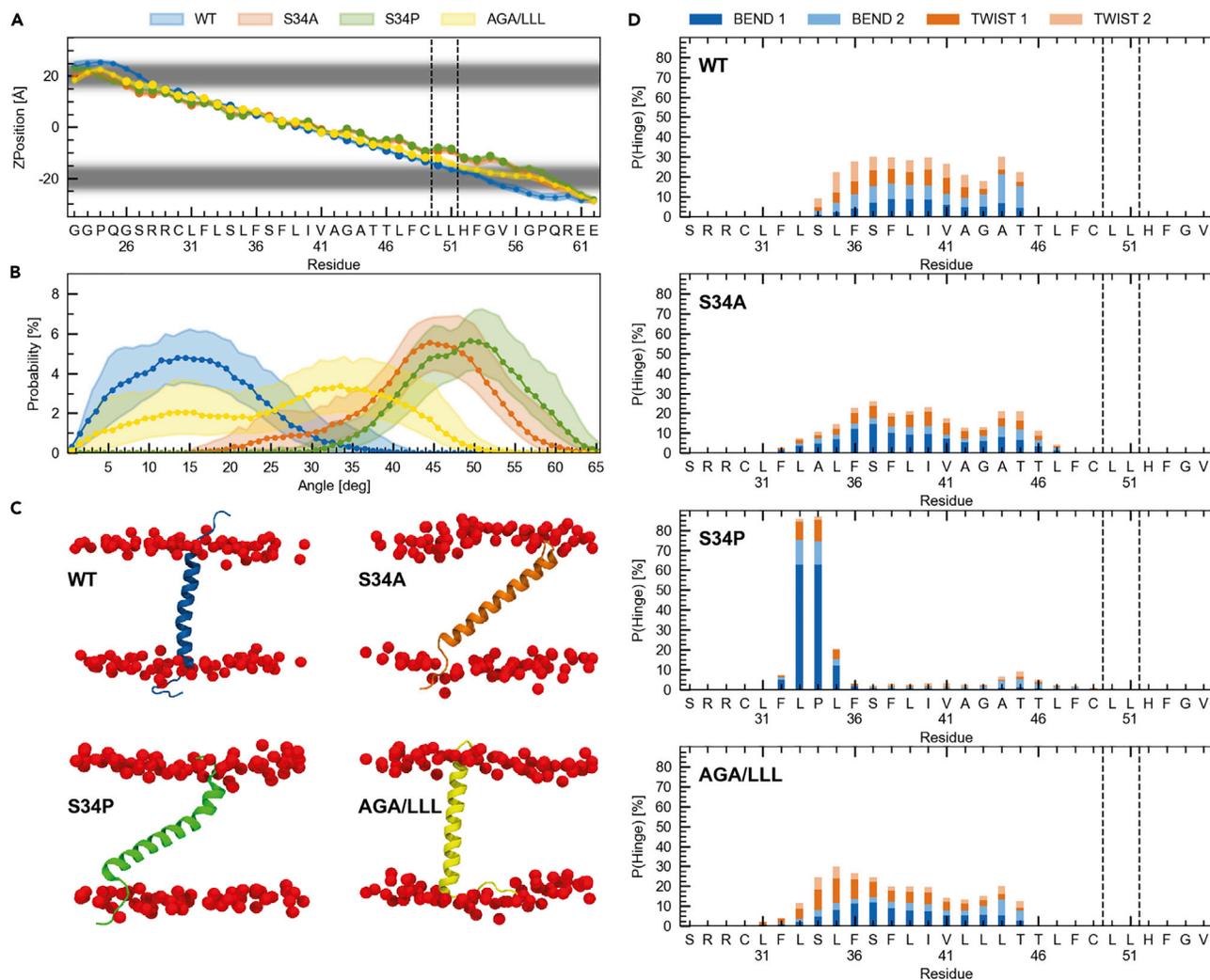
Figure 8. TNFα TM Helix Dynamics in a POPC Bilayer from MD Simulations

(A) Residue insertion depths relative to the lipid phosphate heads. Gray areas represent the location of the phosphate heads. The dots indicate the average Cα position (larger dots specify helical residues as determined by secondary structure analysis, see Figure S7). Dashed lines indicate cleavage sites.

(B) Distribution of tilt angle between the TM-helix (F36-C49) and the membrane normal. The colored areas show the 95% CI.

(C) Representative structures illustrating the orientation in the membrane. Red spheres show lipid phosphates.

(D) Backbone conformations of TNFα wt and mutant TM helices characterized by the probability that a residue is part of a single hinge (types Bend 1, Twist 1) or a pair of hinges (types Bend 2, Twist 2). Dashed lines indicate cleavage sites.

restrict backbone flexibility to low-amplitude bending and twisting (with average screw angles ~10° and root mean-squared fluctuations around the average structure ~0.5 Å) (Figure S7D). Since per-residue hinge propensities <10% are close to the background noise of the applied method, the impact of mutations on preferred backbone conformations can only be roughly characterized. The S34A mutation seems to abrogate twisting over the whole TM helix, while the AGA/LLL mutation appears to preferentially diminish twisting of the C-terminal TM helix part.

Taken together, helix orientation and C-terminal residue insertion in the POPC membrane seem to be dependent on S34. This pronounced distance effect suggests that the hydroxyl group of the N-terminal S34 side chain can act as an anchor for the TNFα TM helix and might even be a key factor for lateral interactions with the enzyme. With the exception of the structural kink induced by the S34P mutant, large deviations from a straight helix are unlikely. H-bonds spanning the region from L35/F36/S37 to L39/I40/V41 show slightly increased flexibility. Instabilities of H-bonds in this region were also detected with DHX and NMR analysis in aqueous TFE solution. A second region of H-bond instabilities is located at the

C-terminal membrane interface close to the initial SPPL2a cleavage sites. In both cases, TM domain flexibility is supported by α- to 3_{10}-H-bond shifting.

DISCUSSION

This study demonstrates a non-canonical shedding activity of SPPL2a on wt TNFα, which was not observed for its close homolog SPPL2b (Figure 1). The latter observation is in line with previous studies, where SPPL2b and presenilins efficiently process only substrates with rather short ECs (Güner and Lichtenthaler, 2020; Martin et al., 2009; Struhl and Greenwald, 1999). In addition, SPP efficiently cleaves signal peptides only after they have been released from nascent secretory or membrane proteins by signal peptidase (Lemberg and Martoglio, 2002). Since SPPL2a and SPPL2b are close homologs and share a very similar cleavage mechanism with presenilin (Figure 2) (Langosch and Steiner, 2017), it was surprising that SPPL2a is capable of processing a substrate with a long and bulky EC. However, SPPL3, a more distant homolog to SPPL2a and SPPL2b (Voss et al., 2013), was recently identified as "bona fide" non-canonical sheddase among GxGD proteases. SPPL3 accepts a number of different glycosyltransferases and glycosidases without prior shedding and, other than SPPL2b, also cleaves the FL foamy virus envelope protein (Kuhn et al., 2015; Voss et al., 2012, 2013). Moreover, it has been recognized that SPP in context of Endoplasmic-reticulum-associated protein degradation (ERAD) assembles into high-molecular-weight complexes, which enables it to act as a "part-time" non-canonical sheddase (Boname et al., 2014; Chen et al., 2014; Hsu et al., 2015; Stagg et al., 2009; Stefanovic-Barrett et al., 2018). Further, presenilins can also process substrates with long ECs, although with rather low efficiency (Boname et al., 2014; Chen et al., 2014; Hsu et al., 2015; Laurent et al., 2015; Lichtenthaler et al., 2018; Schauenburg et al., 2018; Stagg et al., 2009; Stefanovic-Barrett et al., 2018). Interestingly, SPPL3 is the smallest member of the GxGD-protease family, comprising a very short N-terminus and does not undergo glycosylation (Friedmann et al., 2004). Substrate entry into SPPL3 may thus experience the least steric hindrance within the GxGD protease family. In contrast to SPPL3, both SPPL2a and SPPL2b comprise a large and highly glycosylated N-terminal domain, which faces the lumen/extracellular space, but only SPPL2b carries an additional glycosylation site on the loop connecting the active site containing TM domains 6 and 7 (Friedmann et al., 2004). This additional glycosidic chain, which also faces the lumen/extracellular space, may be responsible for the stricter size exclusion of SPPL2b compared to SPPL2a. Other than all SPP/SPPL family members, presenilins associate with three additional membrane proteins (nicastrin, Aph-1, and Pen-2) in a high-molecular-weight γ-secretase complex in order to become fully catalytically active (Prokop et al., 2004). Structural analysis of the γ-secretase complex indicates that nicastrin, which comprises a highly glycosylated ectodomain, forms a lid on top of the active site of presenilin (Bai et al., 2015) and, thus, most likely hinders entry of substrates with bulky ECs to the active site (Bolduc et al., 2016).

In light of SPPL2a acting as a non-canonical sheddase, it may be speculated that, in principle, all GxGD proteases are capable of accepting substrates with rather long ECs to some extent, but protease intrinsic steric properties or the presence of bulky co-factors restrict entry of such substrates. Consequently, non-canonical sheddase efficiency among human GxGD proteases may be ranked as follows:

SPPL3>SPPL2a > SPPL2b > SPP > presenilin

However, to finally proof the proposed hierarchy of non-canonical shedding efficiency, further studies will be required.

SPPL2a non-canonical shedding occurs at the same cleavage sites as hydrolysis of TNFα NTF, which results in the liberation of TNFα C-peptide (Figure 3). However, while the major initial cleavage site in TNFα NTF was mapped at L50, non-canonical shedding of TNFα FL mainly occurred at V55. This may suggest that either binding of TNFα FL to the SPPL2a active site occurs slightly differently than binding of the TNFα NTF. Alternatively, the lack of its bulky EC may position the TNFα NTF in the membrane such that access to the cleavage site at L50 is optimized. Western blot analysis of samples independently treated with SPP/SPPL inhibitor or ADAM10/17 inhibitor (Figure 1) indicated that non-canonical SPPL2a shedding occurs independently from canonical ADAM10/17 shedding of TNFα wt. Although the level of ADAM shedding appeared to be decreased by the G43P mutation in TNFα, we assume that this decrease resulted indirectly from an enhanced SPPL2a processing rate.

Non-canonical TNFα shedding by SPPL2a is greatly facilitated by proline substitutions in the TNFα TM domain. Of note, the strongest increase of non-canonical shedding was achieved by proline substitutions in the N-terminal and central part of the TNFα TM domain (Figure 4). DHX analysis and NMR structural analysis revealed that S34P causes a marked destabilization in the N-terminal part of the TNFα TM domain,

which is predominantly α-helical in TNFα wt (Figure 7). Interestingly, destabilization in the N-terminal part of the TM helix induced increased cleavage by SPPL2a at the C-terminal end of the helix (Figure 5). In line with this, only removal of a potentially helix-destabilizing glycine residue in the N-terminal part of the Bri2 TM domain significantly reduced cleavage by SPPL2b at its C-terminal end, while mutating glycines in the C-terminal part of the Bri2 TM domain had no effect (Fluhrer et al., 2008). In addition, cleavage of CD74 by SPPL2a was reduced by simultaneous substitution of all potentially helix-destabilizing glycine residues in its TM domain. The CD74 TM domain comprises two glycines in the N-terminal part and one in the C-terminal part; however, the role of the individual glycine residues was not investigated (Hüttl et al., 2016).

In order to understand the long-distance effect of S34P, its structure was compared to that of the TNFα wt TM helix by NMR spectroscopy. The TNFα wt TM helix is slightly bent and flexible at its center at an A42/G43/A44 motif where it tends to form a 3_{10} helix (Figures 7 and 8). Bending of the helix is consistent with lower amide H-bond stabilities from T45 to F48, as detected by DHX, which suggests longer amide H-bonds toward residues within the bend. This may reflect an overall curvature of the helix around a central hinge region as indicated by the distributed hinge propensities in a quantitative evaluation of the NOE data (Figure S6) and the NMR conformational ensembles (Figure 7). Similar to TNFα, the G37G38 hinge in the APP TM helix is also distant from the initial ε-cleavage sites of γ-secretase (Götz et al., 2019b). Of note, bending and the deviation from the ideal TM helix geometry in case of TNFα are much less pronounced than for the APP TM helix (Figure 7 ; Silber et al., in press). The S34P mutation strongly destabilizes the N-terminal part of the TM helix and shifts the dominant hinge bending to A42 and G43. Although located distant to the potential hinge region, the S34P mutation resulted in increased H-bond flexibility, as detected by DHX (Figure 6), and a less pronounced bend and, thus, a more linear orientation of N- and C-terminal helix parts (Figure 7). MD simulation of the S34P in a POPC bilayer predicts an increase in the tilt angle of the helix within a lipid bilayer compared to TNFα wt, concomitant with a deeper residue insertion (Figure 8) and a lower percentage of 3_{10}-H-bonds in the region of cleavage (Figure S7). Together with the impact of S34P on the flexibility and positioning of the hinge region, this may explain the long-distance effect observed for cleavage of S34P and likely other proline substitutions in this region.

In contrast, the AGA/LLL substitution strongly reduced non-canonical shedding by SPPL2a (Figure 4) and resulted in a broad helix stabilization from I40 through C49 (Figure 6). This concurs with a shift of the hinge propensity from the center of the TM helix toward T45/T46 that allows for larger bending resulting in a different mutual orientation of the N- and C-terminal part of the helix (Figure 7). However, this did not destabilize downstream amide H-bonds to an extent that was detectable by DHX. These data are reminiscent of previous findings where stabilizing the flexible G37G38 hinge within the APP TM domain by a glycine-to-leucine mutation significantly reduced its cleavage by γ-secretase (Götz et al., 2019b). In addition, reducing the conformational flexibility of the XBP1u TM helix reduced its cleavage by SPP, although increasing helix flexibility had no effect (Yucel et al., 2019).

How do those changes in the structure and dynamics of the TM helix translate into the significantly enhanced non-canonical shedding of S34P and the abolished cleavage of AGA/LLL, respectively (Figure 4)? Our present data and the previous findings on APP indicate that a hinge near the center of a substrate's TM domain may be beneficial for substrate processing. For γ-secretase, substrate processing starts with its recognition at one or more exosites in the γ-secretase complex followed by translocation of the initial cleavage sites to the enzyme's active site, where the substrate docks prior to local unfolding, bond hydrolysis, and product release. It has been proposed that a flexible APP TM helix may be required for multiple steps of processing, in particular for substrate translocation to the catalytic site (Langosch et al., 2015; Langosch and Steiner, 2017). Recent substrate docking experiments indicate transient TM helix kinking at the di-glycine motif of the C99 TM domain during the first step of substrate entry, where the N-terminal part of the helix already occupies its final binding sites while the C-terminal part begins to bypass the cytosolic loop of γ-secretase (Hitzenberger et al., 2020). To finally proof whether these findings fully translate to substrate recognition by SPP/SPPL proteases, the 3D structures of the enzymes will be required.

The major initial cleavage sites at L50 and H52 are located within stable C-terminal helical sections of the TNFα TM domain (Figures 6 and 7). While the S34P or AGA/LLL mutations significantly changed the efficiency of non-canonical shedding (Figure 4), they did not affect the structure or H-bond stability directly at the cleavage site (Figures 6 and 7). Introducing potentially helix-destabilizing C49P or H52P mutations directly at the cleavage site had only a minor or no effect on cleavage efficiency, while introducing a C49L or H52L mutation reduced cleavage efficiency (Figure 4). It is believed that local unfolding of a substrate TM helix at the cleavage site is required for efficient

peptide bond hydrolysis. However, it is currently unclear whether the leucine mutations exert their inhibitory effect via stabilizing the helix around the scissile bond or via interfering with the docking of the substrate into the enzyme. Recent cryo-EM structures for γ-secretase in complex with Notch1 or APP CTF showed that substrate helix unfolding at the initial cleavage sites was induced and stabilized by the formation of a hybrid β-sheet composed of β-strands in PS1 and in the substrate's TM domain, downstream to the initial cleavage sites (Götz et al., 2019a, 2019b). Since, at present, no structural data of any SPP/SPPL family member in complex with a substrate is available, it remains enigmatic whether TNFα undergoes a similar interaction with the enzyme, which induces substrate unfolding. However, based on sequence analysis, the β-strand of PS1 may be conserved in all members of the SPP/SPPL family which suggests a conserved mechanism requiring local substrate docking and unfolding for both protease families, including a requirement for amino acid sequence determinants as it has been discussed for substrate docking to SPP (Lemberg and Martoglio, 2002; Yucel et al., 2019).

Under physiological conditions, SPPL2a-mediated non-canonical TNFα shedding most likely only yields a small amount of total secreted TNFα. Since SPPL2a is mainly active in lysosomes (Schröder et al., 2010), it may be speculated that TNFα FL, which escapes processing by ADAM10/17 on the cell surface, is endocytosed and shed by SPPL2a in the lysosome. To explain subsequent secretion of sTNFα(L2a), sorting in exocytic vesicles similar to, for instance, the LDL receptor (Wijers et al., 2015) may be postulated.

In light of the efficient non-canonical shedding of some of our TNFα mutants, it is tempting to speculate that hitherto unknown physiological type-II TM substrates exist that are primarily cleaved by non-canonical SPPL2a shedding. We suggest the following requirements for these substrates: (i) The TM helix must exhibit flexibility in its N-terminal region and (ii) a flexible hinge region in the N-terminal or central region. We speculate that the profile of backbone flexibility of a substrate TM helix depends on the types of cognate aspartate protease. Possibly, the degree of helix flexibility may match the extent of steric hindrance presented by the enzyme. For example, SPPL2b, which exhibits a greater intrinsic steric hindrance for substrate entry, may require a more pronounced helical flexibility of the substrate's TM domain to overcome this steric barrier. In other words, the more pronounced the steric barrier of the intramembrane protease, the more flexibility in the substrate's TM domain may be required to allow efficient entry of substrates to the active site of the intramembrane protease.

This study identifies a cleavage of SPPL2a in TNFα, which reflects a non-canonical shedding. Thus, a slightly longer TNFα EC is released from the TNFα-expressing cell. Whether this fragment holds different signaling capacities than soluble TNFα produced from canonical ADAM10/17 shedding or simply allows the cell to degrade cell surface TNFα FL that escaped canonical shedding remains to be investigated. By combining cell biology, biochemical, and structural analysis, we provide evidence that non-canonical shedding of SPPL2 substrates is facilitated by flexibility in a part of the TM helix distal to the cleavage site, including a non-linear orientation of its N- and C-terminal parts. The preferred orientation of both parts depends on a flexible hinge in the center of the TM. The position of the hinge in the TM domain depends on sequence context. We expect that an improved understanding of the structure and dynamics of non-canonically shedded GxGD protease substrates will aid their future prediction from primary structure.

Limitations of the Study

At present, the *in vivo* relevance of non-canonical TNFα shedding is not understood. Since TNFα processing in mice seems to be fundamentally different, as multiple fragments released by ADAM-dependent canonical shedding are detectable, it is currently not possible to unambiguously identify SPPL2a-dependent non-canonical shedding in mouse models. In order to identify non-canonical TNFα shedding in human cells reliably, a SPPL2a-deficient macrophage cell line would be needed. Thus, at this stage, the *in vivo* relevance of TNFα non-canonical shedding remains enigmatic.

In addition, it would be of interest whether mutations that alter TNFα non-canonical shedding occur in a physiological or pathophysiological context. However, so far, no TNFα variations have been documented that could account for such processing defects. Single-nucleotide polymorphisms have only been reported in the promotor region of the TNFα gene accounting mostly for altered expression levels.

Resource Availability

Lead Contact

Further information and requests for resources and reagents should be directed to and will be fulfilled by the Lead Contact, Regina Fluhrer (regina.fluhrer@med.uni-augsburg.de).

Materials Availability

Cell lines and cDNA constructs generated in this study will be made available on request, but we may require a payment and/or a completed Materials Transfer Agreement if there is potential for commercial application.

Data and Code Availability

The NMR data sets (atomic coordinates and experimental data) generated during this study are available in the Protein DataBank (https://www.wwpdb.org). WT: 7ASY; S34P: 7AT7; AGALLL: 7ATB.

The scripts underlying the MD simulation data sets, as well as the mass spectrometry data related to the DHX kinetics experiments generated during this study, are available at Mendeley Data Repository, https://doi.org/10.17632/xbkfyvw4xm.1.

The trajectories from molecular dynamic simulations supporting the current study have not been deposited in a public repository because of their size but are available from the corresponding author on request.

METHODS

All methods can be found in the accompanying Transparent Methods supplemental file.

SUPPLEMENTAL INFORMATION

Supplemental Information can be found online at https://doi.org/10.1016/j.isci.2020.101775.

AUTHOR CONTRIBUTIONS

N.G.S. and C.M.G. performed solution NMR. W.S. and D.L. performed DHX and ETD-DHX. S.M., A.G., and C.Scha. performed MD simulation experiments. M.H.-K. performed experiments shown in Figure 2D and provided technical assistance. C.Schl. performed experiments shown in Figures 1F and 1G. C.Sp. performed all other experiments. R.F. conceived the experiments, supervised the project, and wrote the manuscript with input from all authors.

DECLARATION OF INTERESTS

The authors declare no competing interests.

REFERENCES

Bai, X.-C., Yan, C., Yang, G., Lu, P., Ma, D., Sun, L., Zhou, R., Scheres, S.H., and Shi, Y. (2015). An atomic structure of human γ-secretase. Nature *525*, 212–217.

Bardy, S.L., Eichler, J., and Jarrell, K.F. (2003). Archaeal signal peptides–a comparative survey at the genome level. Protein Sci. *12*, 1833–1843.

Barrett, P.J., Song, Y., Van Horn, W.D., Hustedt, E.J., Schafer, J.M., Hadziselimovic, A., Beel,

A.J., and Sanders, C.R. (2012). The amyloid precursor protein has a flexible transmembrane domain and binds cholesterol. Science *336*, 1168–1171.

Black, R.A., Rauch, C.T., Kozlosky, C.J., Peschon, J.J., Slack, J.L., Wolfson, M.F., Castner, B.J., Stocking, K.L., Reddy, P., Srinivasan, S., et al. (1997). A metalloproteinase disintegrin that releases tumour-necrosis factor-alpha from cells. Nature *385*, 729–733.

Bolduc, D.M., Montagna, D.R., Gu, Y., Selkoe, D.J., and Wolfe, M.S. (2016). Nicastrin functions to sterically hinder gamma-secretase-substrate interactions driven by substrate transmembrane domain. Proc. Natl. Acad. Sci. U S A *113*, E509–E518.

Boname, J.M., Bloor, S., Wandel, M.P., Nathan, J.A., Antrobus, R., Dingwell, K.S., Thurston, T.L., Smith, D.L., Smith, J.C., Randow, F., and Lehner, P.J. (2014). Cleavage by signal peptide peptidase

is required for the degradation of selected tail-anchored proteins. J. Cell Biol. *205*, 847–862.

Bowie, J.U. (2011). Membrane protein folding: how important are hydrogen bonds? Curr. Opin. Struct. Biol. *21*, 42–49.

Brenner, D., Blaser, H., and Mak, T.W. (2015). Regulation of tumour necrosis factor signalling: live or let die. Nat. Rev. Immunol. *15*, 362–374.

Cao, Z., and Bowie, J.U. (2012). Shifting hydrogen bonds may produce flexible transmembrane helices. Proc. Natl. Acad. Sci. U S A *109*, 8121–8126.

Chen, C.Y., Malchus, N.S., Hehn, B., Stelzer, W., Avci, D., Langosch, D., and Lemberg, M.K. (2014). Signal peptide peptidase functions in ERAD to cleave the unfolded protein response regulator XBP1u. EMBO J. *33*, 2492–2506.

Cordes, F.S., Bright, J.N., and Sansom, M.S. (2002). Proline-induced distortions of transmembrane helices. J. Mol. Biol. *323*, 951–960.

Ehlers, M.R., and Riordan, J.F. (1991). Membrane proteins with soluble counterparts: role of proteolysis in the release of transmembrane proteins. Biochemistry *30*, 10065–10074.

Fernandez, M.A., Biette, K.M., Dolios, G., Seth, D., Wang, R., and Wolfe, M.S. (2016). Transmembrane substrate determinants for gamma-secretase processing of APP CTFbeta. Biochemistry *55*, 5675–5688.

Fluhrer, R., Fukumori, A., Martin, L., Grammer, G., Haug-Kroper, M., Klier, B., Winkler, E., Kremmer, E., Condron, M.M., Teplow, D.B., et al. (2008). Intramembrane proteolysis of GXGD-type aspartyl proteases is slowed by a familial Alzheimer disease-like mutation. J. Biol. Chem. *283*, 30121–30128.

Fluhrer, R., Grammer, G., Israel, L., Condron, M.M., Haffner, C., Friedmann, E., Bohland, C., Imhof, A., Martoglio, B., Teplow, D.B., and Haass, C. (2006). A gamma-secretase-like intramembrane cleavage of TNFalpha by the GxGD aspartyl protease SPPL2b. Nat. Cell Biol. *8*, 894–896.

Fluhrer, R., Martin, L., Klier, B., Haug-Kroper, M., Grammer, G., Nuscher, B., and Haass, C. (2012). The alpha-helical content of the transmembrane domain of the British dementia protein-2 (Bri2) determines its processing by signal peptide peptidase-like 2b (SPPL2b). J. Biol. Chem. *287*, 5156–5163.

Friedmann, E., Hauben, E., Maylandt, K., Schleeger, S., Vreugde, S., Lichtenthaler, S.F., Kuhn, P.H., Stauffer, D., Rovelli, G., and Martoglio, B. (2006). SPPL2a and SPPL2b promote intramembrane proteolysis of TNFalpha in activated dendritic cells to trigger IL-12 production. Nat. Cell Biol. *8*, 843–848.

Friedmann, E., Lemberg, M.K., Weihofen, A., Dev, K.K., Dengler, U., Rovelli, G., and Martoglio, B. (2004). Consensus analysis of signal peptide peptidase and homologous human aspartic proteases reveals opposite topology of catalytic domains compared with presenilins. J. Biol. Chem. *279*, 50790–50798.

Götz, A., Högel, P., Silber, M., Chaitoglou, I., Luy, B., Muhle-Goll, C., Scharnagl, C., and Langosch, D. (2019a). Increased H-bond stability relates to altered epsilon-cleavage efficiency and abeta levels in the I45T familial alzheimer's disease mutant of APP. Sci. Rep. *9*, 5321.

Götz, A., Mylonas, N., Högel, P., Silber, M., Heinel, H., Menig, S., Vogel, A., Feyrer, H., Huster, D., and Luy, B. (2019b). Modulating hinge flexibility in the APP transmembrane domain alters γ-secretase cleavage. Biophys. J. *116*, 2103–2120.

Götz, A., and Scharnagl, C. (2018). Dissecting conformational changes in APP's transmembrane domain linked to ε-efficiency in familial Alzheimer's disease. PLoS One *13*, e0200077.

Gray, T., and Matthews, B. (1984). Intrahelical hydrogen bonding of serine, threonine and cysteine residues within α-helices and its relevance to membrane-bound proteins. J. Mol. Biol. *175*, 75–81.

Grigorenko, A.P., Moliaka, Y.K., Korovaitseva, G.I., and Rogaev, E.I. (2002). Novel class of polytopic proteins with domains associated with putative protease activity. Biochemistry *67*, 826–835.

Güner, G., and Lichtenthaler, S.F. (2020). The substrate repertoire of γ-secretase/presenilin. Semin. Cell Dev. Biol. *105*, 27–42.

Haass, C., and Steiner, H. (2002). Alzheimer disease gamma-secretase: a complex story of GxGD-type presenilin proteases. Trends Cell Biol. *12*, 556–562.

Hayward, S., and Lee, R.A. (2002). Improvements in the analysis of domain motions in proteins from conformational change: DynDom version 1.50. J. Mol. Graph Model. *21*, 181–183.

Hemming, M.L., Elias, J.E., Gygi, S.P., and Selkoe, D.J. (2008). Proteomic profiling of gamma-secretase substrates and mapping of substrate requirements. PLoS Biol. *6*, e257.

Hitzenberger, M., Gotz, A., Menig, S., Brunschweiger, B., Zacharias, M., and Scharnagl, C. (2020). The dynamics of gamma-secretase and its substrates. Semin. Cell Dev. Biol. *105*, 86–101.

Högel, P., Götz, A., Kuhne, F., Ebert, M., Stelzer, W., Rand, K.D., Scharnagl, C., and Langosch, D. (2018). Glycine perturbs local and global conformational flexibility of a transmembrane helix. Biochemistry *57*, 1326–1337.

Hsu, F., Yeh, C., Sun, Y., Chiang, M., Lan, W., Li, F., Lee, W.-H., and Chau, L.Y. (2015). Signal peptide peptidase-mediated nuclear localization of heme oxygenase-1 promotes cancer cell proliferation and invasion independent of its enzymatic activity. Oncogene *34*, 2360–2370.

Hüttl, S., Helfrich, F., Mentrup, T., Held, S., Fukumori, A., Steiner, H., Saftig, P., Fluhrer, R., and Schröder, B. (2016). Substrate determinants of signal peptide peptidase-like 2a (SPPL2a)-mediated intramembrane proteolysis of the invariant chain CD74. Biochem. J. *473*, 1405–1422.

Kabsch, W., and Sander, C. (1983). Dictionary of protein secondary structure: pattern recognition of hydrogen-bonded and geometrical features. Biopolymers *22*, 2577–2637.

Konermann, L., Pan, J., and Liu, Y.H. (2011). Hydrogen exchange mass spectrometry for studying protein structure and dynamics. Chem. Soc. Rev. *40*, 1224–1234.

Kopan, R., and Ilagan, M.X. (2004). Gamma-secretase: proteasome of the membrane? Nat. Rev. Mol. Cell Biol. *5*, 499–504.

Kuhn, P.-H., Voss, M., Haug-Kröper, M., Schröder, B., Schepers, U., Bräse, S., Haass, C., Lichtenthaler, S.F., and Fluhrer, R. (2015). Secretome analysis identifies novel signal Peptide peptidase-like 3 (Sppl3) substrates and reveals a role of Sppl3 in multiple Golgi glycosylation pathways. Mol. Cell Proteomics *14*, 1584–1598.

Langosch, D., Scharnagl, C., Steiner, H., and Lemberg, M.K. (2015). Understanding intramembrane proteolysis: from protein dynamics to reaction kinetics. Trends Biochem. Sci. *40*, 318–327.

Langosch, D., and Steiner, H. (2017). Substrate processing in intramembrane proteolysis by gamma-secretase - the role of protein dynamics. Biol. Chem. *398*, 441–453.

LaPointe, C.F., and Taylor, R.K. (2000). The type 4 prepilin peptidases comprise a novel family of aspartic acid proteases. J. Biol. Chem. *275*, 1502–1510.

Laurent, S.A., Hoffmann, F.S., Kuhn, P.H., Cheng, Q., Chu, Y., Schmidt-Supprian, M., Hauck, S.M., Schuh, E., Krumbholz, M., Rübsamen, H., et al. (2015). γ-Secretase directly sheds the survival receptor BCMA from plasma cells. Nat. Commun. *6*, 7333.

Lemberg, M.K., and Martoglio, B. (2002). Requirements for signal peptide peptidase-catalyzed intramembrane proteolysis. Mol. Cell *10*, 735–744.

Lichtenthaler, S.F., Lemberg, M.K., and Fluhrer, R. (2018). Proteolytic ectodomain shedding of membrane proteins in mammals-hardware, concepts, and recent developments. EMBO J. *37*, e99456.

Martin, L., Fluhrer, R., and Haass, C. (2009). Substrate requirements for SPPL2b-dependent regulated intramembrane proteolysis. J. Biol. Chem. *284*, 5662–5670.

Martin, L., Fluhrer, R., Reiss, K., Kremmer, E., Saftig, P., and Haass, C. (2008). Regulated intramembrane proteolysis of Bri2 (Itm2b) by ADAM10 and SPPL2a/SPPL2b. J. Biol. Chem. *283*, 1644–1652.

McGeehan, G.M., Becherer, J.D., Bast, R.C., Jr., Boyer, C.M., Champion, B., Connolly, K.M., Conway, J.G., Furdon, P., Karp, S., Kidao, S., et al. (1994). Regulation of tumour necrosis factor-alpha processing by a metalloproteinase inhibitor. Nature *370*, 558–561.

Mentrup, T., Fluhrer, R., and Schroder, B. (2017). Latest emerging functions of SPP/SPPL intramembrane proteases. Eur. J. Cell Biol. *96*, 372–382.

Mentrup, T., Hasler, R., Fluhrer, R., Saftig, P., and Schroder, B. (2015). A cell-based assay reveals nuclear translocation of intracellular domains released by SPPL proteases. Traffic 16, 871–892.

Mentrup, T., Theodorou, K., Cabrera-Cabrera, F., Helbig, A.O., Happ, K., Gijbels, M., Gradtke, A.C., Rabe, B., Fukumori, A., Steiner, H., et al. (2019). Atherogenic LOX-1 signaling is controlled by SPPL2-mediated intramembrane proteolysis. J. Exp. Med. 216, 807–830.

Millhauser, G.L. (1995). Views of helical peptides: a proposal for the position of 310-helix along the thermodynamic folding pathway. Biochemistry 34, 3873–3877.

Mohan, M.J., Seaton, T., Mitchell, J., Howe, A., Blackburn, K., Burkhart, W., Moyer, M., Patel, I., Waitt, G.M., Becherer, J.D., et al. (2002). The tumor necrosis factor-alpha converting enzyme (TACE): a unique metalloproteinase with highly defined substrate selectivity. Biochemistry 41, 9462–9469.

Nagase, H., and Nakayama, K. (2013). gamma-Secretase-regulated signaling typified by Notch signaling in the immune system. Curr. Stem Cell Res. Ther. 8, 341–356.

Nyborg, A.C., Jansen, K., Ladd, T.B., Fauq, A., and Golde, T.E. (2004). A signal peptide peptidase (SPP) reporter activity assay based on the cleavage of type II membrane protein substrates provides further evidence for an inverted orientation of the SPP active site relative to presenilin. J. Biol. Chem. 279, 43148–43156.

Papadopoulou, A.A., Muller, S.A., Mentrup, T., Shmueli, M.D., Niemeyer, J., Haug-Kroper, M., Von Blume, J., Mayerhofer, A., Feederle, R., Schroder, B., et al. (2019). Signal Peptide Peptidase-Like 2c (SPPL2c) impairs vesicular transport and cleavage of SNARE proteins. EMBO Rep. 20, e46451.

Pester, O., Barrett, P.J., Hornburg, D., Hornburg, P., Probstle, R., Widmaier, S., Kutzner, C., Durrbaum, M., Kapurniotu, A., Sanders, C.R., et al. (2013). The backbone dynamics of the amyloid precursor protein transmembrane helix provides a rationale for the sequential cleavage mechanism of gamma-secretase. J. Am. Chem. Soc. 135, 1317–1329.

Ponting, C.P., Hutton, M., Nyborg, A., Baker, M., Jansen, K., and Golde, T.E. (2002). Identification of a novel family of presenilin homologues. Hum. Mol. Genet. 11, 1037–1044.

Poschner, B.C., Quint, S., Hofmann, M.W., and Langosch, D. (2009). Sequence-specific conformational dynamics of model transmembrane domains determines their membrane fusogenic function. J. Mol. Biol. 386, 733–741.

Prokop, S., Shirotani, K., Edbauer, D., Haass, C., and Steiner, H. (2004). Requirement of PEN-2 for

stabilization of the presenilin N-/C-terminal fragment heterodimer within the γ-secretase complex. J. Biol. Chem. 279, 23255–23261.

Quint, S., Widmaier, S., Minde, D., Hornburg, D., Langosch, D., and Scharnagl, C. (2010). Residue-specific side-chain packing determines the backbone dynamics of transmembrane model helices. Biophys. J. 99, 2541–2549.

Sato, C., Morohashi, Y., Tomita, T., and Iwatsubo, T. (2006). Structure of the catalytic pore of gamma-secretase probed by the accessibility of substituted cysteines. J. Neurosci. 26, 12081–12088.

Sato, T., Tang, T.C., Reubins, G., Fei, J.Z., Fujimoto, T., Kienlen-Campard, P., Constantinescu, S.N., Octave, J.N., Aimoto, S., and Smith, S.O. (2009). A helix-to-coil transition at the epsilon-cut site in the transmembrane dimer of the amyloid precursor protein is required for proteolysis. Proc. Natl. Acad. Sci. U S A 106, 1421–1426.

Scharnagl, C., Pester, O., Hornburg, P., Hornburg, D., Götz, A., and Langosch, D. (2014). Side-chain to main-chain hydrogen bonding controls the intrinsic backbone dynamics of the amyloid precursor protein transmembrane helix. Biophys. J. 106, 1318–1326.

Schauenburg, L., Liebsch, F., Eravci, M., Mayer, M.C., Weise, C., and Multhaup, G. (2018). APLP1 is endoproteolytically cleaved by gamma-secretase without previous ectodomain shedding. Sci. Rep. 8, 1916.

Schröder, B.A., Wrocklage, C., Hasilik, A., and Saftig, P. (2010). The proteome of lysosomes. Proteomics 10, 4053–4076.

Silber, M., Hitzenberger, M., Zacharias, M., Muhle-Goll, C. Altered hinge conformations in APP transmembrane helix mutants may affect enzyme-substrate interactions of γ-secretase. ACS Chem. Neuroscience. In press.

So, T., and Ishii, N. (2019). The TNF-TNFR family of Co-signal molecules. Adv. Exp. Med. Biol. 1189, 53–84.

Spera, S., and Bax, A. (1991). Correlations of Cα/β chemical shifts to the protein secondary structure. J. Am. Chem. Soc. 113, 5490–5492.

Stagg, H.R., Thomas, M., Van Den Boomen, D., Wiertz, E.J., Drabkin, H.A., Gemmill, R.M., and Lehner, P.J. (2009). The TRC8 E3 ligase ubiquitinates MHC class I molecules before dislocation from the ER. J. Cell Biol. 186, 685–692.

Stefanovic-Barrett, S., Dickson, A.S., Burr, S.P., Williamson, J.C., Lobb, I.T., Van Den Boomen, D.J., Lehner, P.J., and Nathan, J.A. (2018). MARCH6 and TRC8 facilitate the quality control of cytosolic and tail-anchored proteins. EMBO Rep. 19, e45603.

Stelzer, W., and Langosch, D. (2019). Conformationally flexible sites within the transmembrane helices of amyloid precursor protein and Notch1 receptor. Biochemistry 58, 3065–3068.

Struhl, G., and Greenwald, I. (1999). Presenilin is required for activity and nuclear access of Notch in Drosophila. Nature 398, 522–525.

Voss, M., Fukumori, A., Kuhn, P.-H., Künzel, U., Klier, B., Grammer, G., Haug-Kröper, M., Kremmer, E., Lichtenthaler, S.F., and Steiner, H. (2012). Foamy virus envelope protein is a substrate for signal peptide peptidase-like 3 (SPPL3). J. Biol. Chem. 287, 43401–43409.

Voss, M., Kunzel, U., Higel, F., Kuhn, P.H., Colombo, A., Fukumori, A., Haug-Kroper, M., Klier, B., Grammer, G., Seidl, A., et al. (2014). Shedding of glycan-modifying enzymes by signal peptide peptidase-like 3 (SPPL3) regulates cellular N-glycosylation. EMBO J. 33, 2890–2905.

Voss, M., Schroder, B., and Fluhrer, R. (2013). Mechanism, specificity, and physiology of signal peptide peptidase (SPP) and SPP-like proteases. Biochim. Biophys. Acta 1828, 2828–2839.

Weihofen, A., Binns, K., Lemberg, M.K., Ashman, K., and Martoglio, B. (2002). Identification of signal peptide peptidase, a presenilin-type aspartic protease. Science 296, 2215–2218.

Wijers, M., Kuivenhoven, J.A., and Van De Sluis, B. (2015). The life cycle of the low-density lipoprotein receptor: insights from cellular and in-vivo studies. Curr. Opin. Lipidol. 26, 82–87.

Wishart, D.S., Sykes, B.D., and Richards, F.M. (1991). Relationship between nuclear magnetic resonance chemical shift and protein secondary structure. J. Mol. Biol. 222, 311–333.

Wüthrich, K. (1986). NMR with proteins and nucleic acids. Europhys. News 17, 11–13.

Xiao, H., Hoerner, J.K., Eyles, S.J., Dobo, A., Voigtman, E., Mel'cuk, A.I., and Kaltashov, I.A. (2005). Mapping protein energy landscapes with amide hydrogen exchange and mass spectrometry: I. A generalized model for a two-state protein and comparison with experiment. Protein Sci. 14, 543–557.

Yucel, S.S., Stelzer, W., Lorenzoni, A., Wozny, M., Langosch, D., and Lemberg, M.K. (2019). The metastable XBP1u transmembrane domain defines determinants for intramembrane proteolysis by signal peptide peptidase. Cell Rep. 26, 3087–3099.e11.

Zhou, R., Yang, G., Guo, X., Zhou, Q., Lei, J., and Shi, Y. (2019). Recognition of the amyloid precursor protein by human gamma-secretase. Science 363, eaaw0930.

Supplemental Information

Non-canonical Shedding of TNFα by SPPL2a

Is Determined by the Conformational

Flexibility of Its Transmembrane Helix

Charlotte Spitz, Christine Schlosser, Nadja Guschtschin-Schmidt, Walter Stelzer, Simon Menig, Alexander Götz, Martina Haug-Kröper, Christina Scharnagl, Dieter Langosch, Claudia Muhle-Goll, and Regina Fluhrer
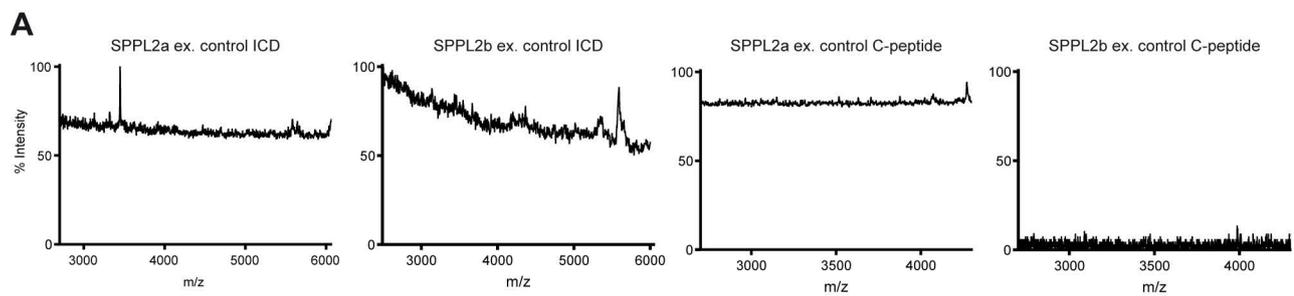
Figure S1: Characterization of SPPL2a/b ko cells, Related to Figure 1
(A) Expression of SPPL2a Crispr generated knock out cell lines. SPPL2a was expressed in wt HEK293 cells but not in newly generated SPPL2a single and SPPL2a and b double knockout cell lines. Expression of SPPL2a was not affected in SPPL2b knockout cell lines. **(B)** Sequencing of newly generated cells lines (left). SPPL2 guide RNA generated a frameshift mutation (left) inducing a premature stop codon (right).

A

B

C-peptide (cleavage position)	predicted (in Da)	measured (in Da)	
		SPPL2a	SPPL2b
60	3045	3044	3041
55	3540	3539	3537
52	3881	3881	3879
51	3987	3993	3982
50	4107	4107	4107

ICD (cleavage position)	predicted (in Da)	measured (in Da)	
		SPPL2a	SPPL2b
18	3058	3059	3059
20	3314	3321	3312
26	3811		3800
27	3889	3892	
28	4055	4056	4050
31	4427	4429	
34	4774	4776	4775
35	4888	4892	
37	5122	5126	5124
39	5383	5383	5383

Figure S2: Empty controls and peak size, Related fo Figure 2

(A) Controls of cell lysate or conditioned media analysed by mass spectrometry. **(B)** Table of predicted and measured peak sizes of TNFα wt construct.

A

B

C-peptide (cleavage position)	predicted (in Da)	measured (in Da)
77	2237	2237
73	2620	2620
69	3031	3031
66	3346	3347
55	4595	4598
52	4937	4940
50	5163	5168
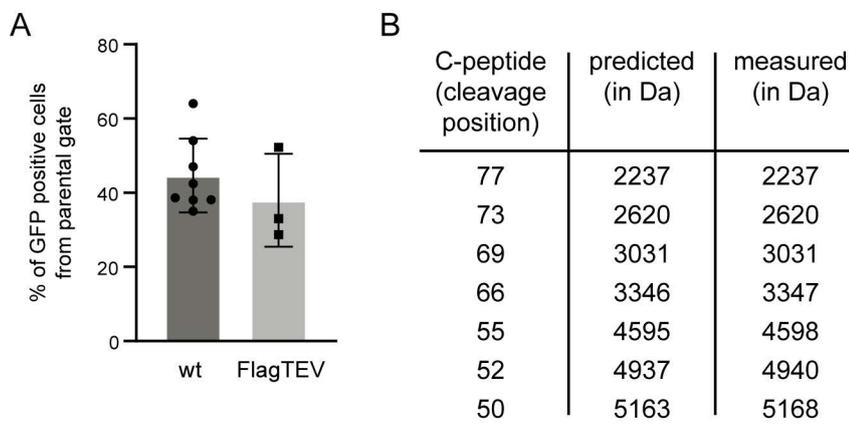
Figure S3: Controls for TNFα Flag TEV construct, Related to Figure 3 **(A)** Surface expression of TNFα wt and TNFα FlagTEV. Cells transiently transfected with the respective constructs were surface stained with V5-mono antibody and then analysed by flow cytometry. GFP positive cells were gated from a single cell population, wt n=8, FlagTEV n=3. Data are represented as mean +/- SD. Statistical significance was calculated applying an unpaired, two-sided Student's t-test. **(B)** Table of predicted and measured peak sizes in TNFα FlagTEV construct.
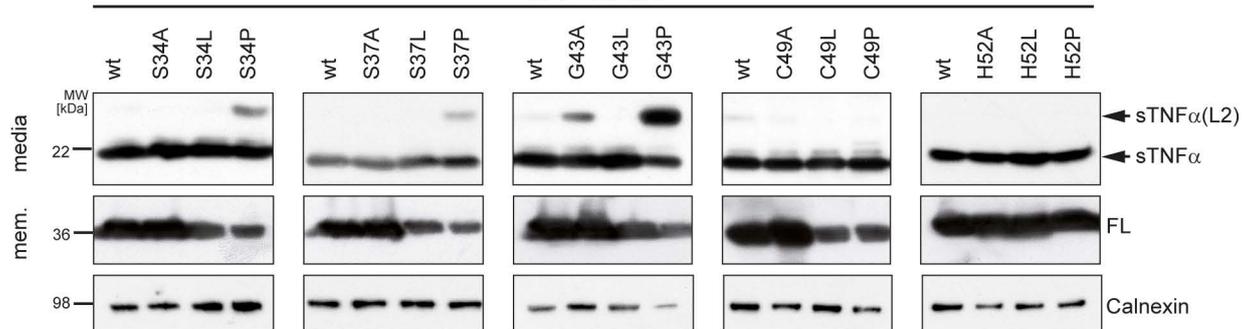
Figure S4: Non-canonical shedding of TNFα mutants by SPPL2b, Related to Figure 4
Mutations in the TM domain of TNFα induce shedding by SPPL2b. In the media of cells co-expressing SPPL2b and the respective TNFα variant, secreted TNFα was detected with a V5-mono antibody. Detection of TNFα FL in the membranes served as transfection and calnexin as loading control.

A

wt: RRC LFLSLFSFLIVAGATTLFCLLHF GVIGPQR
        28   60
S34A: ... ...A....................... ....
S34P: ... ...P....................... ....
AGA/LLL:... ....LLL........... ....

B

C
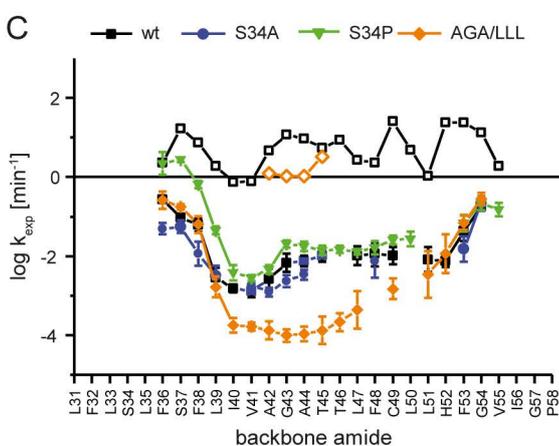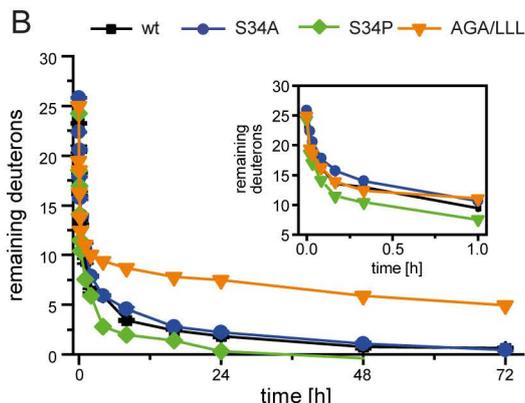
Figure S5: Overall and site-specific DHX of TNFα transmembrane helix variants,
Related to Figure 6

(A) Sequences of TNFα TM domain peptides used for DHX experiments (in the mutant sequences, dots represent wt residues). **(B)** Overall amide DHX kinetics of the TNFα wt TMD peptide compared with mutants recorded at pH 5 and 20°C. The inset details the exchange kinetics within the first hour of incubation (n=3, SEM are smaller than the sizes of the symbols). **(C)** Exchange rate constants kexp of individual amide deuterons (filled symbols, n = 3, log k_{exp} ± error of fit) and chemical exchange rate constants k_{ch} (emtpy symbols). A comparison of the k_{exp} and k_{ch} values, that represent the respective amide-specific intrinsic chemical rate constants and describe the exchange kinetics in the unfolded state (Englander, 2006, Skinner et al., 2012), reveals that the differences between k_{exp} and k_{ch} are stronger at the central region of the helices than at more terminal regions, indicating stronger protection from exchange in their central parts.
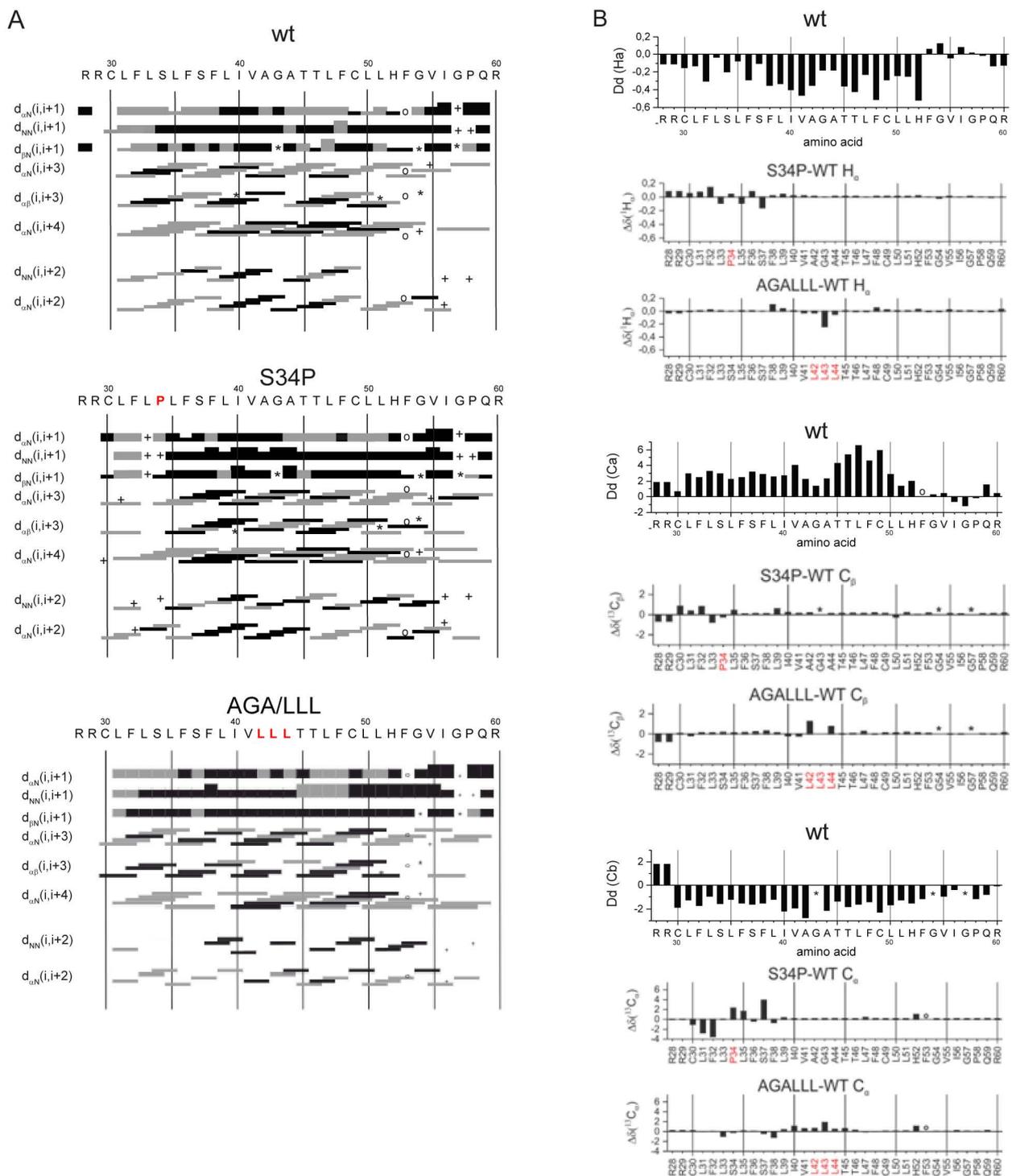
Figure S6: Secondary structure characteristics determined by NMR spectroscopy, Related to Figure 7
(A) Characteristic NOEs of TNFα WT, TNFα S34P and TNFα AGA/LLL. The intensities of the sequential NOEs are proportional to the height of the box; no proportionality is shown for non-sequential contacts. Black boxes indicate unambiguous and grey boxes ambiguous NOEs. Residues marked with asterisk are glycines or contacts to glycines without $^{13}C_\beta$ atoms. + prolines respectively contacts to prolines. ° NOEs to F53 $^1H_\alpha$ could not be observes because of too close proximity to the saturated water resonance at 4.7.
(B) Chemical shift differences between random coil values and TNFα wt, TNFα S34P and TNFα AGA/LLL. Positive $^{13}C_\alpha$ secondary chemical shifts together with negative $^1H_\alpha$ and $^{13}C_\beta$ secondary chemical shifts denote α-helices. *Glycines without $^{13}C_\beta$ atoms. ° The $^{13}C_\alpha$ resonance frequency of F53 could not be determined in the $^1H^{13}C$-HSQC because F53 $^1H_\alpha$ was disturbed by the overlapping water resonance at 4.7.
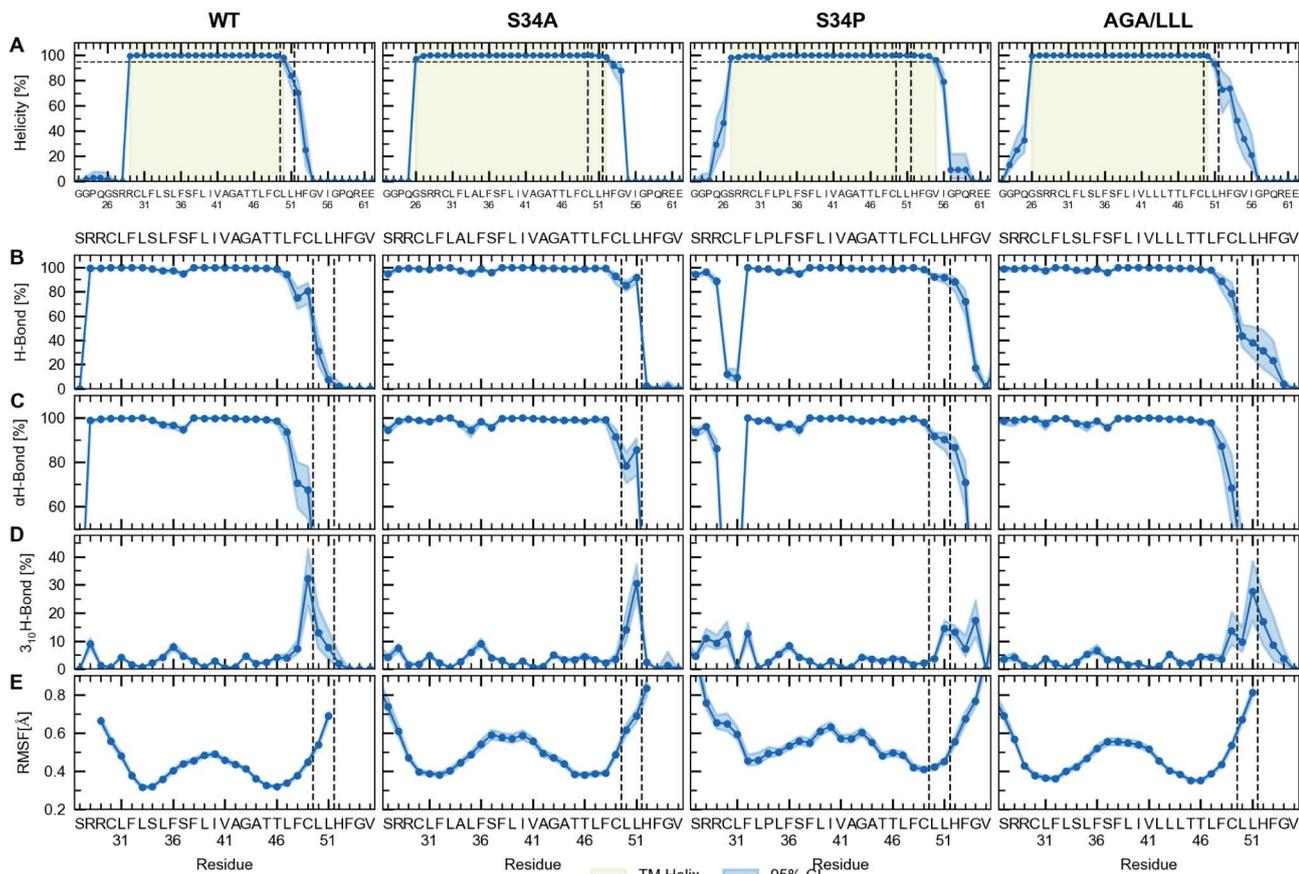
Figure S7: Secondary structure, H-bond occupancies and backbone fluctuations of TNFα wt and mutant TM domains in a POPC bilayer from MD simulations, Related to Figure 8

(A) Secondary structure analysis using the DSSP algorithm (Kabsch and Sander, 1983). A residue is identified as part of the TM helix if its helicity is >95% (beige rectangle). **(B)** Occupancies of α-helical H-bonds between carboxyl O(i) and amide-H(i+4). **(C)** Occupancies of 3_{10}-helical H-bonds between carboxyl O(i) and amide-H(i+3). An H-bond is counted as closed, if (i) the distance between donor hydrogen and the acceptor oxygen is <2.6 Å, and (ii) the O...H-N angle is larger than 120°. **(D)** Root mean-square fluctuations (RMSF) around the average structure of the TM helix. Colored areas indicate 95% CI. Initial cleavage sites are marked with dashed lines.

Table S1: ETD D/H exchange data, Related to Figure 6

Numerical values of k_{exp} and ΔG

	wt[1]		amide	S34A		amide	S34P		amide	AGA/LLL	
amide	log k_{exp} [3] [min^{-1}]	ΔG [4] [kcal/mol]		log k_{exp} [min^{-1}]	ΔG [kcal/mol]		log k_{exp} [min^{-1}]	ΔG [kcal/mol]		log k_{exp} [min-1]	ΔG [kcal/mol]
R29	n.d.[2]		•	n.d.		•	n.d.		•	n.d.	
C30	n.d.		•	n.d.		•	n.d.		•	n.d.	
L31	n.d.		•	n.d.		•	n.d.		•	n.d.	
F32	n.d.		•	n.d.		•	n.d.		•	n.d.	
L33	n.d.		•	n.d.		•	n.d.		•	n.d.	
S34	n.d.		A	n.d.		P	--		•	n.d.	
L35	n.d.		•	n.d.		•	n.d.		•	n.d.	
F36	-0.57 ± 0.07	1.2 ± 0.10	•	-1.31 ± 0.15	2.2 ± 0.20	•	0.34 ± 0.28	(-2.1 ± 2.2)	•	-0.59 ± 0.22	1.2 ± 0.34
S37	-1.03 ± 0.09	3.0 ± 0.11	•	-1.25 ± 0.16	3.3 ± 0.22	•	0.44 ± 0.06	1.0 ± 0.17	•	-0.75 ± 0.06	2.7 ± 0.08
F38	-1.21 ± 0.17	2.8 ± 0.22	•	-1.94 ± 0.31	3.8 ± 0.41	•	-0.19 ± 0.09	1.4 ± 0.19	•	-1.20 ± 0.21	2.8 ± 0.29
L39	-2.54 ± 0.25	3.8 ± 0.34	•	-2.51 ± 0.26	3.7 ± 0.35	•	-1.34 ± 0.10	2.2 ± 0.19	•	-2.78 ± 0.26	4.1 ± 0.35
I40	-2.81 ± 0.10	3.6 ± 0.13	•	n.d.		•	-2.42 ± 0.19	3.1 ± 0.30	•	-3.74 ± 0.18	4.8 ± 0.25
V41	-2.88 ± 0.15	3.7 ± 0.20	•	-2.73 ± 0.09	3.5 ± 0.13	•	-2.56 ± 0.08	3.3 ± 0.14	•	-3.78 ± 0.10	4.9 ± 0.14
A42	-2.58 ± 0.27	4.3 ± 0.36	•	-2.91 ± 0.11	4.8 ± 0.15	•	-2.33 ± 0.11	4.0 ± 0.23	L	-3.88 ± 0.23	5.3 ± 0.31
G43	-2.17 ± 0.23	4.3 ± 0.31	•	-2.63 ± 0.15	5.0 ± 0.20	•	-1.69 ± 0.09	3.7 ± 0.24	L	-4.01 ± 0.16	5.4 ± 0.22
A44	-2.13 ± 0.13	4.3 ± 0.18	•	-2.47 ± 0.13	4.6 ± 0.18	•	-1.75 ± 0.12	3.6 ± 0.20	L	-3.97 ± 0.18	5.3 ± 0.25
T45	-1.99 ± 0.14	3.6 ± 0.19	•	n.d.		•	-1.86 ± 0.12	3.5 ± 0.21	•	-3.88 ± 0.35	5.9 ± 0.46
T46	n.d.		•	n.d.		•	-1.84 ± 0.09	3.7 ± 0.18	•	-3.67 ± 0.23	6.2 ± 0.31
L47	-1.99 ± 0.24	3.2 ± 0.32	•	n.d.		•	-1.89 ± 0.07	3.1 ± 0.15	•	-3.36 ± 0.48	5.1 ± 0.64
F48	-1.94 ± 0.31	3.1 ± 0.42	•	-2.13 ± 0.42	3.3 ± 0.57	•	-1.79 ± 0.17	2.9 ± 0.23	•	n.d.	
C49	-1.99 ± 0.22	4.6 ± 0.29	•	n.d.		•	-1.59 ± 0.11	4.0 ± 0.30	•	-2.83 ± 0.27	5.7 ± 0.36
L50	n.d.		•	n.d.		•	-1.57 ± 0.19	3.0 ± 0.44	•	n.d.	
L51	-2.08 ± 0.31	2.8 ± 0.42	•	n.d.		•	n.d.		•	-2.47 ± 0.59	3.3 ± 0.80
H52	-2.13 ± 0.15	4.7 ± 0.20	•	n.d.		•	n.d.		•	-1.94 ± 0.49	4.4 ± 0.66
F53	-1.36 ± 0.26	3.7 ± 0.35	•	-1.82 ± 0.32	4.3 ± 0.43	•	-1.17 ± 0.21	3.4 ± 0.34	•	-1.15 ± 0.18	3.4 ± 0.24
G54	-0.75 ± 0.11	2.5 ± 0.15	•	-0.67 ± 0.18	2.4 ± 0.26	•	-0.68 ± 0.17	2.4 ± 0.23	•	-0.55 ± 0.16	2.2 ± 0.22
V55	n.d.		•	n.d.		•	-0.82 ± 0.16	1.4 ± 0.27	•	n.d.	
I56	n.d.		•	n.d.		•	n.d.		•	n.d.	
G57	n.d.		•	n.d.		•	n.d.		•	n.d.	
P58	--		•	--		•	--		•	--	
Q59	n.d.		•	n.d.		•	n.d.		•	n.d.	
R60	n.d.		•	n.d.		•	n.d.		•	n.d.	

[1] Identity of the TMD peptide

[2] n.d. = not determined

[3] k_{exp} from exponential fit of means ± SE

[4] ΔG with confidence interval

Transparent methods

Molecular cloning and cDNA constructs

The cDNAs that encode SPPL2a and SPPL2b and a C-terminal HA-tag have been described earlier (Martin et al., 2008). TNFα wt and TNFα NTF comprise N-terminal Flag and a C-terminal V5 tags and have been described earlier (Fluhrer et al., 2008). Mutated TNFα cDNAs were either cloned via quick change PCR or purchased at IDT. After the starting methionine an N-terminal FLAG tag (DYKDDDDK) and, at the C-terminus of the protein, a V5 tag (GKPIPNPLLGLDST) were added. The PCR products or gBlocks were subcloned into the HindIII and XhoI sites of a pcDNA3.1 Hygro(+) vector (Life Technologies, Hennigsdorf). For MALDI TOF analysis tags were swapped, the V5 tag was added N-terminally and a FlagAP tag (DYKDDDDKAP) C-terminally (TNFα NTF-AP).

TNFα Flag-TEV was designed by adding a Flag Tag and a TEV cleavage site (ENLYFQG) one helix turn (4 AA) after the ADAM cleavage site at position 77. All primer sequences are available upon request, and all expression constructs were sequence-verified prior to experimental use.

Cell lines and cell culture

T-Rex™-293 (HEK293) (Invitrogen, Hennigsdorf, Germany) were cultured in DMEM with Glutamax (Invitrogen, Hennigsdorf, Germany) supplemented with 10% fetal calf serum (Sigma), 1% penicillin/streptomycin (Gibco) and 5µg/ml Blasticidin (Invitrogen, Hennigsdorf, Germany).

HEK293 cells stably expressing ectopic SPPL2a or SPPL2b have been described earlier (Martin et al., 2008). Of note, these cells endogenously express SPPL2a and low levels of SPPL2b. Cells were cultured in DMEM with Glutamax (Invitrogen, Hennigsdorf, Germany) supplemented with 10% fetal calf serum (Sigma), 1% penicillin/streptomycin (Gibco), 5µg/ml Blasticidin (Invitrogen, Hennigsdorf, Germany) and 10 µg/ml Zeocine (Invitrogen, Hennigsdorf, Germany). To induce expression of the SPPL2 constructs, cells were incubated with 1 µg/ml

doxycycline (BD Biosciences, San Jose) added to an otherwise antibiotic free medium at least 24 h before transient transfection of the SPPL2 substrates. Transient transfections of cells were carried out using Lipofectamine 2000 (Invitrogen, Hennigsdorf, Germany) according to the manufacturer's instructions. To inhibit protease function inhibitors were added into the culture media for 24h ((Z-LL)$_2$ ketone, ADAM inhibition: GI254023X, Merck, Darmstadt, BMS-561392, provided kindly by Haass Lab).

Generation of knock out cells

Guide RNAs targeting the SPPL2a or SPPL2b gene were purchased from Sigma-Aldrich (Darmstadt, Germany; 01111718MN, 11091608MN). For SPPL2a two human GFP-tagged guide RNAs both binding in exon 1 were tested. SPPL2b GFP-tagged guide RNA was chosen to bind in exon 4 to target all different splice variants. HEK293 cells were transiently transfected with the respective guide RNAs and submitted to FACS based single cell sorting and sorted for their GFP signal. Protease knockdowns were validated with PCR followed by sequencing and SPPL2a knockdown was additionally confirmed on protein level using Western Blot analysis. SPPL2a/b double knockout was achieved by transfecting HEK293 SPPL2b knockout cells with SPPL2a guide RNA. Validation was carried out as for the single SPPL2a knock out cell line. Potential off target effects were excluded using NCBI Nucleotide BLAST.

Membrane isolation, immunoprecipitation and immunoblotting

Cells were harvested on ice and lysed in ice-cold hypoton buffer (10mM Tris, 1mM EDTA, 1mM EGTA, pH 7.6) supplemented with protease inhibitor mix (1:500) (P1860, Sigma Aldrich, Darmstadt, Germany). Membranes were isolated by centrifugation at 16.000 x g and resuspended in basic buffer (40mM Tris,40mM potassium acetate, 1.6mM magnesium acetate, 100mM sucrose, 0.8mM DTT). Samples were incubated as indicated in the respective figure. Subsequently proteins were precipitated with chloroform/ methanol (2:1) and resuspended in sample buffer (10% (v/v) glycerol, 7.5% (w/v) SDS, 7.5% (w/v) DTT, traces of bromophenol blue, dissolved in 4x upper Tris (0,5M Tris, 0,8% (w/v) SDS pH6.8)). For

immunoprecipitation cells were harvested on ice and lysed in ice-cold STE buffer (150 mM NaCl, 50 mM Tris (pH 7.6), and 2mM EDTA) supplemented with 1% (v/v) NP-40, 1% (v/v) Triton X-100 and protease inhibitor mix (1:500). Anti-Flag® M2 affinity gel (Sigma-Aldrich, Darmstadt, Germany) was used to precipitate TNFα FL and all intracellular cleavage products. Secreted ectodomains were precipitated from conditioned media using V5 polyclonal AB3792 (Thermo Fisher, Hennigsdorf, Germany) and protein G sepharose beads (GE Healthcare, Solingen, Germany). Isolated proteins were washed 3 times with STEN lysis buffer (50mM Tris HCl ph7.6, 150mM NaCl, 2mM EDTA pH 8, 0.2µM NP-40), sample buffer was added, and samples were incubated 10 min at 95°C.

For separation of intracellular TNFα species and TNFα C-peptides a modified Tris-Tricine gel was used (Fluhrer et al., 2006). Secreted TNFα ectodomain species were separated on 12% SDS-PAGE. Samples were blotted on PVDF or – for cleavage products smaller than 6 kDa - on nitrocellulose membranes. Blocking unspecific antibody binding was performed by using a commercial kit (Thermo Fisher, Hennigsdorf, Germany) according to the manufacturer's instructions. Primary antibodies (Flag M2®, Sigma-Aldrich, Darmstadt, Germany, V5 monoclonal R960-25, Invitrogen, Hennigsdorf, Germany, SPPL2a 6E9, (Voss et al., 2012)) as indicated in the respective figures were incubated overnight at 4°C, secondary antibodies were added 1h at RT, Blots were detected using PierceTM ECL Western Blotting Substrate (Thermo Fisher, Hennigsdorf, Germany) or Westar Antares (Cyanagen, Bologna, Italy).

Mass Spectrometry

Secreted protein species were precipitated as described above. Isolated peptides were washed 3x with MS-washing buffer (0,14M NaCl, 0,1% N-octyleglycopyranoside, 10mM Tris-HCl pH 7,6, 5mM EDTA) and 2x with dH$_2$O. For detection of cleavage sites in TNFα FlagTEV the isolated peptides were eluted from the beads with 100mM glycine pH 2.5 and cleaved with AcTEV according to the manufacture's instructions (Invitrogen, Hennigsdorf, Germany). The cleaved peptides were precipitated with Flag Agarose for 1h followed by 3 washes with MS-washing buffer and 2 washes with dH$_2$O. For ICD detection, membranes were incubated for

45 min at 37 °C, solubilized in SPP stock buffer (50mM Tris HCl ph7.8, 50mM potassium acetate, 2mM magnesium acetate, 125mM sucrose, 1mM DTT) supplemented with 2% DDM and incubated 30 min on ice before centrifugation at 16.000 x g. Peptides were immunoprecipitated using Anti-Flag® M2 affinity gel. Immunoprecipitates were washed 3 times with MS-washing buffer and twice with dH_2O. Samples were subjected to analysis by mass spectrometry using a α-cyano-4-hydroxycinnamic acid matrix (Sigma Aldrich, Darmstadt, Germany) mixed 1:1 with acetonitrile and 0,6% TFA. Three times 0,4 µl of sample was spotted on a 384 spot plate and left to dry at room temperature. Mass spectra were recorded on a 4800 MALDI TOF/TOF analyzer (Applied Biosystems, Hennigsdorf, Germany) in the linear mode with external calibration.

Peptide synthesis

Peptides for D/H exchange (DHX) comprising AA 28 to 60 of TNFα were synthesized by Fmoc chemistry (PSL, Heidelberg, Germany or Zhengzhou Peptides Pharmaceutical Technology Co., Ltd., Zhengzhou, China) and purified by HPLC. Purity was > 90% as judged by mass spectrometry. Concentrations were determined via UV spectroscopy using an extinction coefficient at 205 nm of 142 900 $M^{-1} \cdot cm^{-1}$. All other chemicals were obtained from Sigma-Aldrich Co. (St. Louis, Missouri, USA).

For solution NMR experiments N-terminal acetylation and C-terminal amidation of TNFα28-60 was used. TNFα wt, S34P, and AGA/LLL peptides were purchased from the Core Unit Peptid-Technologien, University of Leipzig, Germany, with a purity of >90 % as judged by mass spectrometry.

Deuterium/Hydrogen exchange experiments and Electron Transfer Dissociation D/H-exchange

Prior to DHX and Electron Transfer Dissociation D/H-exchange (ETD-DHX) peptides were deuterated in 80% (v/v) d1-HFIP/20% D_2O at a concentration of 300 µM and incubated at 37°C for 7 days. To avoid contamination with dissolved polypropylene from reaction tubes, glass

inserts were used in 1.5 ml safe-lock tubes. After 7 days, the solution was put in a new reaction tube and the solvent was removed by SpeedVac centrifugation. The remaining peptide pellet was dissolved in 80% (v/v) d1-TFE in 2 mM ND_4-acetate. Deuterated dithiothreitol (DTT) (prepared by repeated dissolution of DTT in D_2O, overnight lyophilization and dissolving the deuterated DTT in D_2O) was used at a final concentration of 1 mM to reduce the disulfide bridges of the cysteines in the deuterated samples. This prevents considerable dimerization of the peptides by disulfide bonds upon prolonged storage in TFE and HFIP as was detected by mass spectrometry. Finally the deuteration level was > 95%.

For global DHX measurements, the deuterated peptides were diluted 1:20 from a 100 µM deuterated peptide stock solution in 80% (v/v) TFE in 2 mM NH_4-acetate (+ 0.5 mM tris(2-carboxyethyl)phosphine (TCEP)), pH 5.0 (peptide final concentration: 5 µM) and incubated for different time periods (t = 0,1 min, 2 min, 5 min, 10 min, 20 min, 1 h, 2 h, 4h, 8 h, 16 h, 24 h, 48 h, 72 h) in 0.5 ml Eppendorf safe-lock tubes (Eppendorf, Germany) at 20°C in a thermal cycler (MasterCycler from Eppendorf, Germany). To slow down the exchange reaction before measurement, samples were quenched by putting them on ice and adding formic acid (0.5% (v/v) final concentration) which lowered the pH to ≈2.5. Mass/charge (m/z) ratios were recorded after the indicated time periods using a Synapt G2 HDMS mass spectrometer (Waters Co., Milford, MA) with one scan/second. The calculation of equilibrium constants was done for a standard situation of exchange in pure water. The absolute values obtained for K_{eq} may thus be overestimated due to a number of factors as detailed elsewhere (Stelzer et al., 2016). Nonetheless, these factors influence DHX of all TMDs tested in a similar fashion, thus, allowing their comparison.

For ETD-DHX measurement, a solution of deuterated peptide (100 µM) was diluted 1:20 with protonated solvent (80% (v/v) TFE in 2 mM NH_4-acetate (+ 1 mM TCEP), pH 5.0 (standard pH 5.0 or other pH values) to a final peptide concentration of 5 µM and incubated at 20°C in a thermal cycler (MasterCycler® from Eppendorf, Germany). 10-11 different incubation times

from 0.1 min at pH 4 (corresponding to 1 min at pH 5.0) up to 3.95 h at pH 6.5 (corresponding to 125 h at pH 5.0) were applied. ETD was conducted by injecting the cooled and quenched peptide samples with a 100 µl gas-tight Hamilton syringe (a flow rate: 5 µl/min) and a short PEEK-tubing with a needle port. During the measurement, the syringe was cooled down by a -20°C cool pack. The ETD MS/MS measurements were carried out in sensitivity mode. As ETD reagent 1,4- dicyanobenzene was used, which was delivered by a flow of nitrogen gas (makeup flow: 30 ml/min). The glow discharge ion source was operated at 60 µA, with refill times of 100 ms between 1 s MS/MS scans. The selection window for MS/MS mode was ± 2.0 m/z units. The trap T-Wave ion guide was operated with a wave height of 0.2 V and a wave velocity of 300 m/s. Spectra were measured over 10 min in the range of m/z 50 – 3500 by selecting the 5+ charged peptides as MS/MS precursor for ETD. Further parameters were: capillary voltage (2.8 kV), sampling cone (20-22 V), extraction cone (2.0 V), source temperature (90°C), desolvation gas temperature (300°C), cone gas (0 L/h), desolvation gas (800 L/h), transfer collision voltage (5.0) and gas control (trap 14 ml/min and transfer 0.3 ml/min). ETD was started by decreasing the wave height voltage from 1.5 V to 0.2 V. All experiments were done at least in triplicate. For ETD spectra data evaluation, the ETD Fragment Analyzer module of the software suite MassMap® (MassMap GmbH & Co. KG, Wolfratshausen, Germany) was used. It is based on GRAMS/AI (Thermo Fisher Scientific, Waltham (MA), USA). ETD spectra over 10 min were combined and evaluated as described in detail previously (Yucel et al., 2019).

Molecular dynamics (MD) simulations

TNFα22-62 WT, TNFα22-62 S34A, TNFα22-62 S34P and TNFα22-62 AGA/LLL model peptides with neutral termini were analysed in a fully hydrated POPC bilayer. Because no experimental structures were available for the TNFα WT TM domain and the mutants, we used a stochastic sampling protocol to generate a set of start conformations (for details, see (Gotz et al., 2019). The sampled conformations were hierarchically clustered, and the centroid of the cluster with the highest population was placed in a symmetric bilayer, consisting of 128 POPC

lipids (90waters/lipid, ionic strength), using protocols as provided by CHARMM-GUI (Lee et al., 2016). Simulations of 2 µs length (T = 303.15 K, p = 0.1 MPa, integration time step 2fs) were performed using GROMACS 2019.3 (Berendsen et al., 1995). Frames were recorded every 10 ps. Only the last 1 µs of the trajectory were subjected to analysis. All simulations use the CHARMM36 force field (Best et al., 2012). Analysis of the H-bond occupancies and helix tilt angles were performed as described in our previous work (Gotz et al., 2019, Götz et al., 2019). For secondary structure analysis, we used the DSSP algorithm (Kabsch and Sander, 1983). Helix backbone conformations and location of hinge regions were analysed with the program Dyndom (Hayward and Lee, 2002). A straight helix was used as a reference structure for the analysis of the conformational ensembles from NMR and MD. This reference was determined from the average structure of the TNFα22-62 WT peptide in POPC. For structural visualization in Figs 8 and Supp 7 Visual Molecular Dynamics was used (Humphrey et al., 1996).

Solution NMR

Dry TNFα28-60 wt, S34P and AGA/LLL peptides were dissolved in 500 µL HFIP, 5 mM TCEP was added to reduce potential disulfide bridges and the pH was adjusted between 4 to 5 by adding NaOH. The solvent was removed by lyophilization and the dry peptide film was dissolved in 500 µL 80% TFE-d2 and 20% dH$_2$O with renewed addition of 5 mM TCEP. The pH was finally adjusted to 6.5. Peptide concentration ranged between 2 to 4 mg/mL (500 µM to 1 mM).

NMR spectra of peptides were recorded on a 600 MHz AVANCE III spectrometer (Bruker BioSpin, Rheinstetten, Germany) equipped with a TXI cryoprobe at a temperature of 303 K. To assign ^{1}H and ^{13}C-resonances of the peptides a set of two-dimensional spectra was recorded: ^{1}H-^{1}H-TOCSY with a mixing time of 60 ms, ^{1}H-^{1}H-NOESY with a mixing time of 200 ms and natural abundance ^{1}H-^{13}C-HSQC. Spectra were recorded with 48 scans and 1000 data points in the indirect dimension. ^{1}H and 13C chemical shifts are referenced to TFE. The NMR spectra were processed with TopSpin 3.5 pl 7 (Bruker BioSpin, Rheinstetten, Germany) and analyzed using CcpNmr Analysis (Vranken et al., 2005). Dihedral restraints for Φ and Ψ

backbone dihedral angles were derived from chemical shift data using the program TALOS+ (Shen et al., 2009). All structure calculations were performed with CNS(Brunger et al., 1998) using the ARIA2 setup (Rieping et al., 2007). PyMOL (http://www.pymol.org) was used to visualize the protein structures.

Supplemental References

BERENDSEN, H. J., VAN DER SPOEL, D. & VAN DRUNEN, R. 1995. GROMACS: a message-passing parallel molecular dynamics implementation. *Computer physics communications,* 91**,** 43-56.

BEST, R. B., ZHU, X., SHIM, J., LOPES, P. E., MITTAL, J., FEIG, M. & MACKERELL, A. D., JR. 2012. Optimization of the additive CHARMM all-atom protein force field targeting improved sampling of the backbone phi, psi and side-chain chi(1) and chi(2) dihedral angles. *J Chem Theory Comput,* 8**,** 3257-3273.

BRUNGER, A. T., ADAMS, P. D., CLORE, G. M., DELANO, W. L., GROS, P., GROSSE-KUNSTLEVE, R. W., JIANG, J. S., KUSZEWSKI, J., NILGES, M., PANNU, N. S., READ, R. J., RICE, L. M., SIMONSON, T. & WARREN, G. L. 1998. Crystallography & NMR system: A new software suite for macromolecular structure determination. *Acta Crystallogr D Biol Crystallogr,* 54**,** 905-21.

ENGLANDER, S. W. 2006. Hydrogen exchange and mass spectrometry: A historical perspective. *J Am Soc Mass Spectrom,* 17**,** 1481-1489.

FLUHRER, R., FUKUMORI, A., MARTIN, L., GRAMMER, G., HAUG-KROPER, M., KLIER, B., WINKLER, E., KREMMER, E., CONDRON, M. M., TEPLOW, D. B., STEINER, H. & HAASS, C. 2008. Intramembrane proteolysis of GXGD-type aspartyl proteases is slowed by a familial Alzheimer disease-like mutation. *J Biol Chem,* 283**,** 30121-8.

FLUHRER, R., GRAMMER, G., ISRAEL, L., CONDRON, M. M., HAFFNER, C., FRIEDMANN, E., BOHLAND, C., IMHOF, A., MARTOGLIO, B., TEPLOW, D. B. & HAASS, C. 2006. A gamma-secretase-like intramembrane cleavage of TNFalpha by the GxGD aspartyl protease SPPL2b. *Nat Cell Biol,* 8**,** 894-6.

GOTZ, A., HOGEL, P., SILBER, M., CHAITOGLOU, I., LUY, B., MUHLE-GOLL, C., SCHARNAGL, C. & LANGOSCH, D. 2019. Increased H-Bond Stability Relates to Altered epsilon-Cleavage Efficiency and Abeta Levels in the I45T Familial Alzheimer's Disease Mutant of APP. *Sci Rep,* 9**,** 5321.

GÖTZ, A., MYLONAS, N., HÖGEL, P., SILBER, M., HEINEL, H., MENIG, S., VOGEL, A., FEYRER, H., HUSTER, D. & LUY, B. 2019. Modulating hinge flexibility in the APP transmembrane domain alters γ-secretase cleavage. *Biophysical journal,* 116**,** 2103-2120.

HAYWARD, S. & LEE, R. A. 2002. Improvements in the analysis of domain motions in proteins from conformational change: DynDom version 1.50. *J Mol Graph Model,* 21**,** 181-3.

HUMPHREY, W., DALKE, A. & SCHULTEN, K. 1996. VMD: visual molecular dynamics. *Journal of molecular graphics,* 14**,** 33-38.

KABSCH, W. & SANDER, C. 1983. Dictionary of protein secondary structure: pattern recognition of hydrogen-bonded and geometrical features. *Biopolymers,* 22**,** 2577-637.

LEE, J., CHENG, X., SWAILS, J. M., YEOM, M. S., EASTMAN, P. K., LEMKUL, J. A., WEI, S., BUCKNER, J., JEONG, J. C., QI, Y., JO, S., PANDE, V. S., CASE, D. A., BROOKS, C. L., 3RD, MACKERELL, A. D., JR., KLAUDA, J. B. & IM, W. 2016. CHARMM-GUI Input Generator for NAMD, GROMACS, AMBER, OpenMM, and CHARMM/OpenMM Simulations Using the CHARMM36 Additive Force Field. *J Chem Theory Comput,* 12**,** 405-13.

MARTIN, L., FLUHRER, R., REISS, K., KREMMER, E., SAFTIG, P. & HAASS, C. 2008. Regulated intramembrane proteolysis of Bri2 (Itm2b) by ADAM10 and SPPL2a/SPPL2b. *J Biol Chem,* 283**,** 1644-52.

RIEPING, W., HABECK, M., BARDIAUX, B., BERNARD, A., MALLIAVIN, T. E. & NILGES, M. 2007. ARIA2: automated NOE assignment and data integration in NMR structure calculation. *Bioinformatics,* 23**,** 381-2.

SHEN, Y., DELAGLIO, F., CORNILESCU, G. & BAX, A. 2009. TALOS+: a hybrid method for predicting protein backbone torsion angles from NMR chemical shifts. *J Biomol NMR,* 44**,** 213-23.

SKINNER, J. J., LIM, W. K., BÉDARD, S., BLACK, B. E. & ENGLANDER, S. W. 2012. Protein dynamics viewed by hydrogen exchange. *Protein Science,* 21**,** 996-1005.

STELZER, W., SCHARNAGL, C., LEURS, U., RAND, K. D. & LANGOSCH, D. 2016. The impact of the 'Austrian'mutation of the amyloid precursor protein transmembrane helix is communicated to the hinge region. *ChemistrySelect,* 1**,** 4408-4412.

VOSS, M., FUKUMORI, A., KUHN, P.-H., KÜNZEL, U., KLIER, B., GRAMMER, G., HAUG-KRÖPER, M., KREMMER, E., LICHTENTHALER, S. F. & STEINER, H. 2012. Foamy virus envelope protein is a substrate for signal peptide peptidase-like 3 (SPPL3). *Journal of Biological Chemistry,* 287**,** 43401-43409.

Supplement References

BERENDSEN, H. J., VAN DER SPOEL, D. & VAN DRUNEN, R. 1995. GROMACS: a message-passing parallel molecular dynamics implementation. *Computer physics communications,* 91**,** 43-56.

BEST, R. B., ZHU, X., SHIM, J., LOPES, P. E., MITTAL, J., FEIG, M. & MACKERELL, A. D., JR. 2012. Optimization of the additive CHARMM all-atom protein force field targeting improved sampling of the backbone phi, psi and side-chain chi(1) and chi(2) dihedral angles. *J Chem Theory Comput,* 8**,** 3257-3273.

BRUNGER, A. T., ADAMS, P. D., CLORE, G. M., DELANO, W. L., GROS, P., GROSSE-KUNSTLEVE, R. W., JIANG, J. S., KUSZEWSKI, J., NILGES, M., PANNU, N. S., READ, R. J., RICE, L. M., SIMONSON, T. & WARREN, G. L. 1998. Crystallography & NMR system: A new software suite for macromolecular structure determination. *Acta Crystallogr D Biol Crystallogr,* 54**,** 905-21.

FLUHRER, R., FUKUMORI, A., MARTIN, L., GRAMMER, G., HAUG-KROPER, M., KLIER, B., WINKLER, E., KREMMER, E., CONDRON, M. M., TEPLOW, D. B., STEINER, H. & HAASS, C. 2008. Intramembrane proteolysis of GXGD-type aspartyl proteases is slowed by a familial Alzheimer disease-like mutation. *J Biol Chem,* 283**,** 30121-8.

FLUHRER, R., GRAMMER, G., ISRAEL, L., CONDRON, M. M., HAFFNER, C., FRIEDMANN, E., BOHLAND, C., IMHOF, A., MARTOGLIO, B., TEPLOW, D. B. & HAASS, C. 2006. A gamma-secretase-like intramembrane cleavage of TNFalpha by the GxGD aspartyl protease SPPL2b. *Nat Cell Biol,* 8**,** 894-6.

GOTZ, A., HOGEL, P., SILBER, M., CHAITOGLOU, I., LUY, B., MUHLE-GOLL, C., SCHARNAGL, C. & LANGOSCH, D. 2019. Increased H-Bond Stability Relates to Altered epsilon-Cleavage Efficiency and Abeta Levels in the I45T Familial Alzheimer's Disease Mutant of APP. *Sci Rep,* 9**,** 5321.

GÖTZ, A., MYLONAS, N., HÖGEL, P., SILBER, M., HEINEL, H., MENIG, S., VOGEL, A., FEYRER, H., HUSTER, D. & LUY, B. 2019. Modulating hinge flexibility in the APP transmembrane domain alters γ-secretase cleavage. *Biophysical journal,* 116, 2103-2120.

HAYWARD, S. & LEE, R. A. 2002. Improvements in the analysis of domain motions in proteins from conformational change: DynDom version 1.50. *J Mol Graph Model,* 21**,** 181-3.

HUMPHREY, W., DALKE, A. & SCHULTEN, K. 1996. VMD: visual molecular dynamics. *Journal of molecular graphics,* 14**,** 33-38.

KABSCH, W. & SANDER, C. 1983. Dictionary of protein secondary structure: pattern recognition of hydrogen-bonded and geometrical features. *Biopolymers,* 22**,** 2577-637.

LEE, J., CHENG, X., SWAILS, J. M., YEOM, M. S., EASTMAN, P. K., LEMKUL, J. A., WEI, S., BUCKNER, J., JEONG, J. C., QI, Y., JO, S., PANDE, V. S., CASE, D. A., BROOKS, C. L., 3RD, MACKERELL, A. D., JR., KLAUDA, J. B. & IM, W. 2016. CHARMM-GUI Input Generator for NAMD, GROMACS, AMBER, OpenMM, and CHARMM/OpenMM Simulations Using the CHARMM36 Additive Force Field. *J Chem Theory Comput,* 12**,** 405-13.

MARTIN, L., FLUHRER, R., REISS, K., KREMMER, E., SAFTIG, P. & HAASS, C. 2008. Regulated intramembrane proteolysis of Bri2 (Itm2b) by ADAM10 and SPPL2a/SPPL2b. *J Biol Chem,* 283**,** 1644-52.

RIEPING, W., HABECK, M., BARDIAUX, B., BERNARD, A., MALLIAVIN, T. E. & NILGES, M. 2007. ARIA2: automated NOE assignment and data integration in NMR structure calculation. *Bioinformatics,* 23**,** 381-2.

SHEN, Y., DELAGLIO, F., CORNILESCU, G. & BAX, A. 2009. TALOS+: a hybrid method for predicting protein backbone torsion angles from NMR chemical shifts. *J Biomol NMR,* 44**,** 213-23.

STELZER, W., SCHARNAGL, C., LEURS, U., RAND, K. D. & LANGOSCH, D. 2016. The impact of the 'Austrian'mutation of the amyloid precursor protein transmembrane helix is communicated to the hinge region. *ChemistrySelect,* 1**,** 4408-4412.

VOSS, M., FUKUMORI, A., KUHN, P.-H., KÜNZEL, U., KLIER, B., GRAMMER, G., HAUG-KRÖPER, M., KREMMER, E., LICHTENTHALER, S. F. & STEINER, H. 2012. Foamy virus envelope protein is a substrate for signal peptide peptidase-like 3 (SPPL3). *Journal of Biological Chemistry,* 287, 43401-43409.

VRANKEN, W. F., BOUCHER, W., STEVENS, T. J., FOGH, R. H., PAJON, A., LLINAS, M., ULRICH, E. L., MARKLEY, J. L., IONIDES, J. & LAUE, E. D. 2005. The CCPN data model for NMR spectroscopy: development of a software pipeline. *Proteins,* 59**,** 687-96.

YUCEL, S. S., STELZER, W., LORENZONI, A., WOZNY, M., LANGOSCH, D. & LEMBERG, M. K. 2019. The Metastable XBP1u Transmembrane Domain Defines Determinants for Intramembrane Proteolysis by Signal Peptide Peptidase. *Cell Rep,* 26**,** 3087-3099 e11.

VRANKEN, W. F., BOUCHER, W., STEVENS, T. J., FOGH, R. H., PAJON, A., LLINAS, M., ULRICH, E. L., MARKLEY, J. L., IONIDES, J. & LAUE, E. D. 2005. The CCPN data model for NMR spectroscopy: development of a software pipeline. *Proteins,* 59**,** 687-96.

YUCEL, S. S., STELZER, W., LORENZONI, A., WOZNY, M., LANGOSCH, D. & LEMBERG, M. K. 2019. The Metastable XBP1u Transmembrane Domain Defines Determinants for Intramembrane Proteolysis by Signal Peptide Peptidase. *Cell Rep,* 26**,** 3087-3099 e11.